AD-A083 690 DEFENCE RESEARCH ESTABLISHMENT OTTAWA (ONTARIO) F/G 10/3
INVESTIGATION OF CADMIUM SELENIDE PHOTOELECTROCHEMICAL CELLS.(U)
JAN 80 R A SAWCHUK, D R SHELLING
UNCLASSIFIED DREO-TN-804 NL

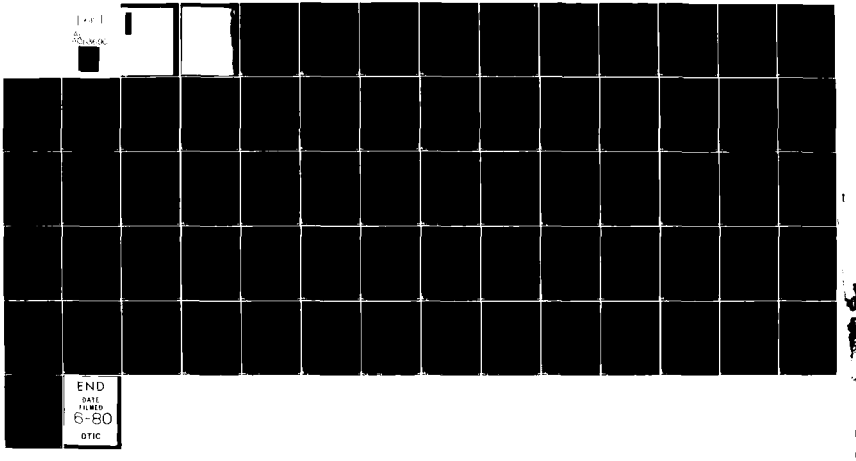

END
DATE FILMED
6-80
DTIC

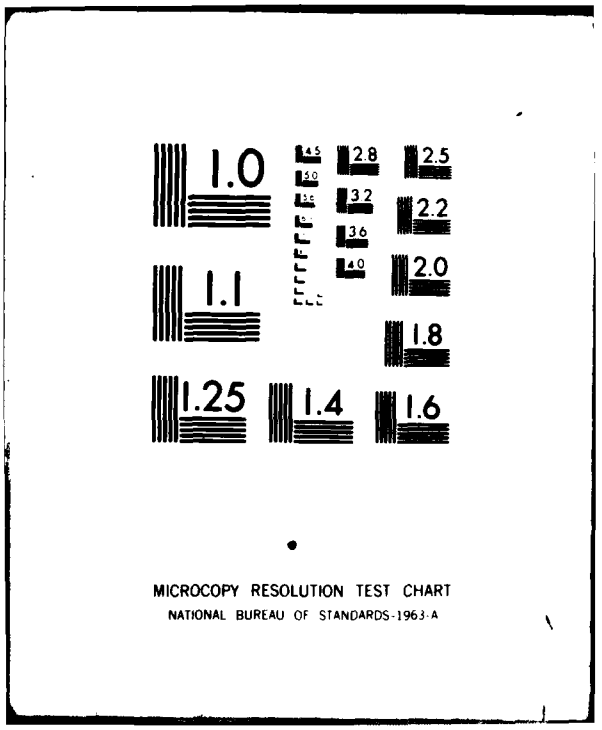
1.0
1.1
1.25
1.4
1.6
1.8
2.0
2.2
2.5
2.8
3.2
3.6
4.0
MICROCOPY RESOLUTION TEST CHART
NATIONAL BUREAU OF STANDARDS-1963-A

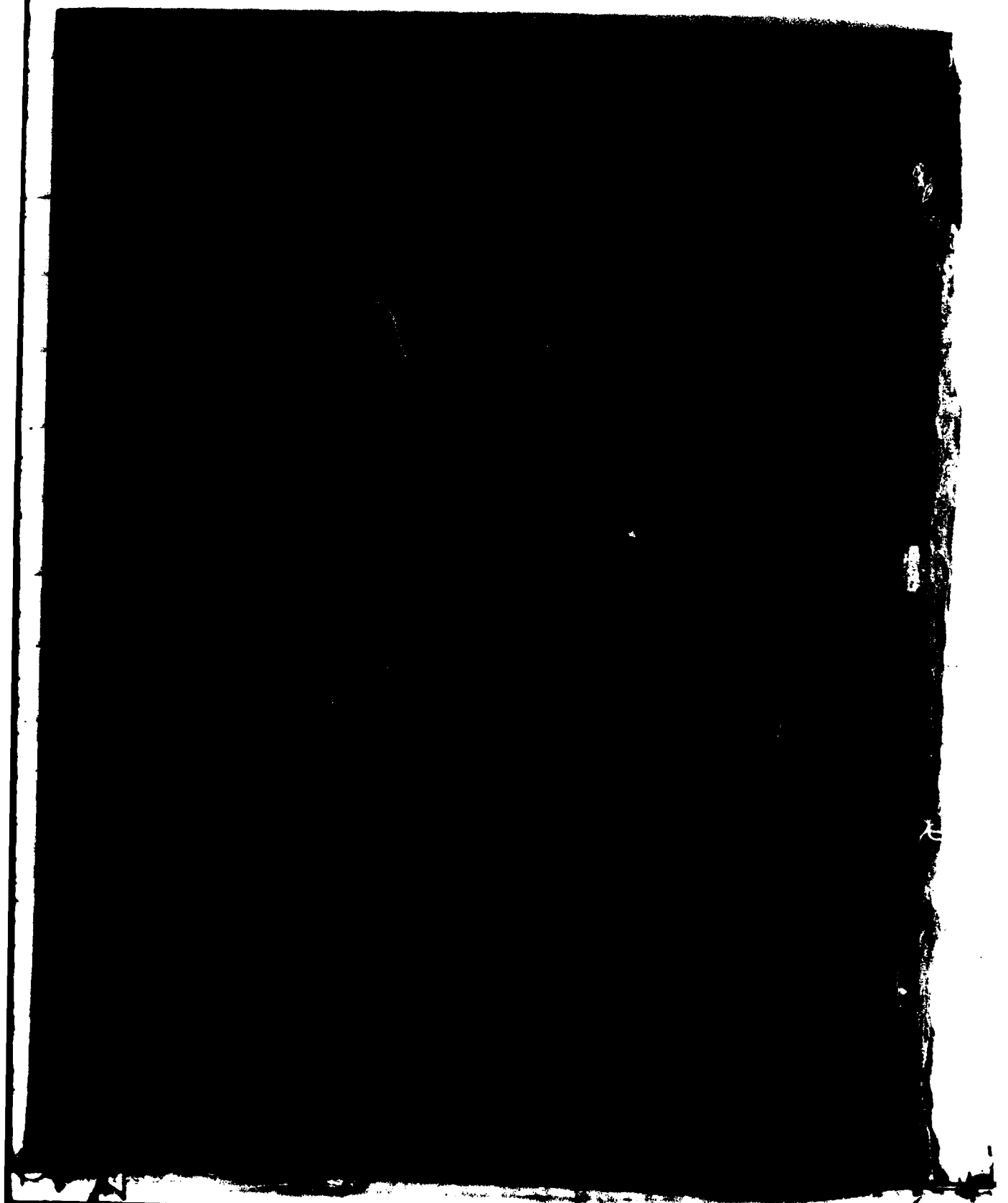

RESEARCH AND DEVELOPMENT BRANCH

DEPARTMENT OF NATIONAL DEFENCE
CANADA

DEFENCE RESEARCH ESTABLISHMENT OTTAWA

(9) TECHNICAL NOTE NO. 80-4

(14) DREO TN 80-4

(6) INVESTIGATION OF CADMIUM SELENIDE PHOTOELECTROCHEMICAL CELLS

by

R.A. Sawchuk and D.R. Snelling
Energy Systems Section
Energy Conversion Division

(10) Robert A. Sawchuk
David R. Snelling

(12) 69

(11) JAN 1980
OTTAWA

404 376

JCB

ABSTRACT

Three photoelectrochemical devices, developed at Simon Fraser University, employing electrochemically deposited cadmium selenide photoanodes, a polysulphide redox electrolyte and an in situ energy storage compartment were evaluated at DREO. The photoelectrochemical devices were initially tested using tungsten filament lamps, and the evaluation was completed with a xenon lamp which closely matched a solar spectrum corresponding to AM1 (air mass 1) conditions having an irradiance level of 889 Wm^{-2}.

Maximum power output of the devices was in the 10-20 mW range resulting in a solar (AM1) to electrical conversion efficiency of < 1%. A fill-factor approaching 0.25 was typical for the photoelectrochemical cells examined. Counter electrode polarization and electrolyte light absorption were identified and evaluated as efficiency limiting factors. Proposed loss mechanisms are: series resistance in the semiconductor bulk, electron tunneling to surface states, current carrier losses at electron-hole recombination centers, and shorting to the nickel substrate. The concept of in situ energy storage was not successfully demonstrated.

It is concluded that counter electrode polarization can be overcome and that further research is required in order to detect the presence of surface states and electron-hole recombination centers, as well as research oriented to characterize the structure of the depletion layer and the CdSe/electrolyte interface. The efficiency of the electrochemically deposited CdSe should approach the 5-10% efficiency observed for single crystal and pressure sintered CdSe.

RÉSUMÉ

Trois cellules photoélectrochimiques, mises au point à l'université Simon Fraser, comportant des photoanodes au séléniure de cadmium déposé électrochimiquement, un électrolyte redox polysulfuré et un compartiment de stockage d'énergie *in situ* ont été examinés au C.R.D.O. Ces cellules ont d'abord été expérimentées à l'aide de lampes à filament de tungstène et on a utilisé par la suite une lampe au xénon émettant un rayonnement de composition spectrale très comparable à celle de la lumière solaire correspondant à des conditions MA1 (masse de l'air 1) et présentant un flux lumineux de 88.9 W/m^2.

La puissance de sortie maximale de ces cellules était comprise entre 10 et 20 mW, donnant ainsi un rendement de conversion de l'énergie solaire en énergie électrique de < 1%. Les cellules photoélectrochimiques étudiées présentaient un facteur de saturation caractéristique de presque 0.25. La polarisation de la contre-électrode ainsi que l'absorption de lumière par l'électrolyte ont été identifiées et considérées comme des facteurs limitant le rendement. Les mécanismes proposés pour expliquer les pertes sont: résistance série dans la masse du semiconducteur, transition d'électrons en effet de tunnel aux états de surface, pertes de porteurs du courant aux centres de recombinaison électrons-trous et court-circuit au substrat de nickel. On n'a pas réussi à démontrer avec succès la notion de stockage de l'énergie *in situ*.

En conclusion: le problème dû à la polarisation de la contre-électrode peut être surmonté; il y a lieu d'effectuer d'autres recherches afin de déceler les états de surface et les centres de recombinaison électrons-trous, ainsi que d'autres études en vue de caractériser la structure de la couche d'épuisement et l'interface CdSe/électrolyte. Le rendement du dépôt électrochimique de CdSe devrait correspondre à peu près au rendement de 5-10% observé pour un cristal unique et pour du CdSe fritté sous pression.

TABLE OF CONTENTS

	Page
ABSTRACT	iii
RÉSUMÉ	iv
TABLE OF CONTENTS	v
ACKNOWLEDGEMENTS	vii
INTRODUCTION	1
EXPERIMENTAL	4
RESULTS	6
EVALUATION OF PHOTOELECTROCHEMICAL CELLS A AND B	6
PHOTOCONVERSION EFFICIENCY	6
ELECTRODE POTENTIAL MEASUREMENTS	20
IN SITU ENERGY STORAGE	24
EVALUATION OF SERIES C PHOTOELECTROCHEMICAL CELLS	28
PHOTOCONVERSION EFFICIENCY	28
ELECTRODE POTENTIAL MEASUREMENTS	33
PHOTOELECTRODE SATURATION EFFECTS	38
HELIUM/NEON LASER PROBE MEASUREMENTS	38
ELECTROLYTE ANALYSIS	44
DISCUSSION	52
CONCLUSIONS AND RECOMMENDATIONS	58
REFERENCES	59

ACKNOWLEDGEMENTS

The authors wish to thank Julia Lewis and Mike Farrington for their assistance in the evaluation of the photoelectrochemical devices. Both of the above were students of the Department of Chemistry, Carleton University, on thesis and project work at DREO under a special arrangement through the Adjunct Professorship at Carleton held by the Division Director, Dr. E.J. Casey. Miss Lewis was supported in part by the Ontario Career Assistance Program at DREO.

INTRODUCTION

In 1977 work was begun by a group headed by Dr. B.L. Funt at Simon Fraser University to develop a cadmium selenide (CdSe) photoelectrochemical cell under a contract administered by the Defence Research Establishment Ottawa (DREO) but supported by funds obtained from federal energy program 1.8. This contract called for the delivery of a device which was to be evaluated at DREO. With this requirement in mind, and since it was anticipated that some similar in-house work would also be initiated, apparatus required to test the photoelectrochemical cells was designed and assembled.

The photoelectrochemical cell (PEC) consists of a semiconductor photoelectrode, a redox electrolyte and a counter electrode. The band bending at the semiconductor/electrolyte boundary leads to potentials which separate the electron/hole pairs produced by photon absorption. Thus the semiconductor/electrolyte boundary takes the place of the p-n junction in the familiar silicon solar cell. The photocurrent is carried by redox reactions occurring at the electrode/electrolyte interface.

The concept of these photoelectrochemical cells (PEC or liquid junction solar cells) is not new. However, cells which show promise of efficient power conversion and stability were only developed in the last few years. The cells are potentially cheap to fabricate since the photoelectrodes can be simply produced, e.g. by electrochemical deposition. Furthermore storage of the converted energy is possible, in situ, with the addition of a storage electrode. The major hurdles to be overcome before these devices can be exploited are their low power conversion efficiencies and their lack of long term stability.

The PEC's developed at Simon Fraser University and reported on here have a CdSe photoanode which is formed by the electrochemical deposition of CdSe on a nickel substrate. The redox electrolyte is polysulphide (sulphur dissolved in 1M $NaOH/Na_2S$) and the counter electrode (cathode) is cobalt treated carbon. In order to meet the requirement of in situ energy storage the photoelectrochemical cells utilized a Ag/Ag_2S storage electrode immersed in an electrolyte comprised of 1M NaOH and 1M Na_2S. A schematic representation of the CdSe photoelectrochemical cells is shown in Figure 1. Key factors in the design of the PEC's are outlined in the following text. Cadmium selenide is an appropriate semiconductor material since its band gap (1.7 eV) falls near the optimum (1.4 eV) for terrestrial-solar to electrical conversion efficiency. The polysulphide redox system not only results in no net chemical change in the electrolyte while sustaining the photocurrent but also serves to stabilize the photoanode. The potential of the redox couple is such that oxidation of the polysulphide species occurs rather than

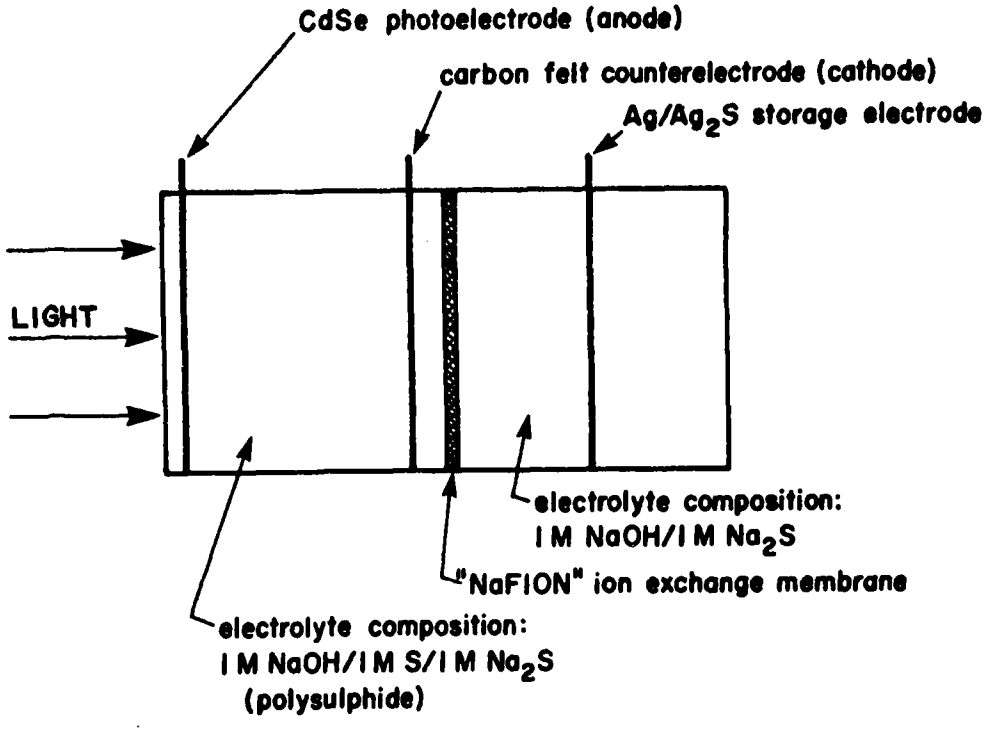

REACTIONS

Photoelectrode: $2h^{+} + 2S^{2-} \longrightarrow S_2^{2-}$

Counterelectrode: $S_2^{2-} + 2e^{-} \longrightarrow 2S^{2-}$

Storage electrode: $Ag_2S + 2e^{-} \underset{\text{discharge}}{\overset{\text{charge}}{\rightleftharpoons}} 2Ag^{\bullet} + S^{2-}$

Fig. 1: Schematic representation of n-type CdSe photoelectrochemical cells.

oxidation of the semiconductor. A cheap and inert carbon felt, doped with cobalt salts to reduce the overpotential, is employed as a counter electrode. The oxidation and reduction of the polysulphide electrolyte involves equilibria such as:

$$aS_n^{2-} + bS_{n-1}^{2-} + cS_{n-2}^{2-} + \cdots \rightleftharpoons \alpha S_n^{2-} + \beta S_{n-1}^{2-} + \gamma S_{n-2}^{2-} + \cdots$$

where the coefficients n, a, b, c, α, β, γ will depend upon the concentration of S, Na_2S and NaOH. Conceptually, the process can be represented by the reaction outlined in Figure 1. The storage of the energy released by photon absorption occurs with the reduction of the Ag_2S to elemental silver and sulphide ions. Subsequently, upon discharging, the energy is recovered by the oxidation of silver yielding Ag_2S. The storage compartment is separated from the polysulphide compartment by an ion exchange membrane.

Photoelectrochemical cells were received for evaluation in the spring of 1978 and in January 1979 as a result of the contracts for FY 77-78 and 78-79, respectively. The two cells received in the spring of 1978 will be referred to as cell A and cell B and the multiple cells, received in January of 1979, as cell C, collectively. A detailed description of the design, fabrication, and assembly of these cells can be found in the final reports to the Department of Supply and Services (ref. 1 for cells A and B, ref. 2 for cell C).

In order to evaluate the solar power conversion efficiencies of the PEC it is necessary to have a light source of known intensity whose spectral distribution matches that of the sun. The extraterrestrial solar intensity at the average sun-earth distance (the solar constant) is 1352 W/m^2. However, for terrestrial applications it is the energy that reaches the ground which is important. The irradiance at ground level depends on solar elevation and atmospheric conditions. The atmosphere absorbs solar radiation (e.g. by H_2O, O_3, CO_2 and other minor constituents) and scatters solar radiation (e.g. Rayleigh and aerosol scattering). The path length through the atmosphere is normally expressed by the number of air masses traversed where unit air mass (AM1) corresponds to an overhead sun. Thus AM2 corresponds to a solar zenith angle of 60° and AM0 corresponds to the extraterrestrial condition. There is a considerable amount of literature on the calculation of atmospheric attenuation and some attempts to quantify the problem require elaborate mathematical models and a great deal of computer time. The simpler approach developed by Thekaekara [3] was adopted. A standard AM1 spectrum with total atmospheric water content of 20 mm, ozone of 3.4 mm, and values of α and β (see ref. 3) of 0.66 and 0.085 respectively, (corresponding to a moderate to high degree of atmospheric aerosols) was adopted. These conditions correspond to a total ground level irradiance of 889.2 W/m^2. Further details on this standard distribution are given in the text. There appears to be no standard spectral distribution which is widely adopted although Brandhorst et al [4] have proposed AM2 with water and ozone values of 20 and 2.4 mm respectively and $\alpha = 1.3$ and $\beta = 0.04$ (clear conditions).

Computer programs have been written to calculate solar spectra using the approach outlined in ref. 3. A description of the technique used,

the computer programs developed and the results obtained will be described separately [5]. A description of the technique can also be found in ref. 4.

The band-gap of CdSe occurs at 730 nm (1.7 eV) and only light of wavelengths shorter than this can excite electrons. Since the solar spectrum is very weak in radiation shorter than 300 nm then the range of wavelengths over which the sun's output should be matched is 300 to 730 nm. In this region the solar spectrum is approximately that of a black-body at 5800 K.

A xenon lamp was chosen for the simulated solar source since its spectral output approximates the solar spectrum, particularly in the range of interest, 300 to 800 nm. Various infrared (IR) filters were used both to improve this match and to reduce the IR heat load on the device being studied.

Since the photoelectrochemical cells were available at the same time that test equipment was being ordered it was necessary to perform some of the tests with equipment which was on hand or could be quickly procured. Conventional tungsten filament lamps, which were readily available, have an equivalent colour balance of approximately 3000 K. Thus the tungsten filament lamp has a spectral output which peaks further to the red than the solar spectrum.

A brief description of the various light sources used and their calibration will be included in the experimental section of this report. A more detailed description will be published separately [5].

EXPERIMENTAL

The light sources used in the PEC evaluations include a 250 W tungsten filament (quartz-halogen type) projector lamp with reflector (General Electric Model ENH Quartzline lamp), an Osram 500 W xenon lamp (Model No. XBO 500 W/h ofr) and a calibrated 200 W quartz-halogen standard lamp (NRC calibrated lamp Nos. QI 111 and Q 112 and lamp M-236 calibrated by the Optronic Laboratories). A brief description of the calibration procedures will be given here and a more complete description will be given separately [5].

A monochromator-detector combination which consisted of either a PRA model B204 monochromator fitted with an EMI 9785B photomultiplier or a GCA McPherson model 218 monochromator equipped with an Optikon PIN-10 UV silicon photodiode was used. The photomultiplier allowed calibration in the range 300 to 800 nm and with the silicon photodiode the wavelength calibration was extended from 800 nm to 1000 nm. Light from the standard lamp was reflected off a MgO coated $MgCO_3$ block in order to fill the field of view of the monochromator. The output from the light sources to be calibrated was measured with a similar configuration.

The basic light sources which were used in the PEC evaluation were as follows: (1) Source No. 1 was the single 250 W quartz-halogen lamp with no filtering or associated optics. (2) Since source 1 did not provide uniform illumination over the 12 cm x 16 cm area of the largest PEC, a second source (No. 2) was built having 4 of the 250 W lamps arranged in a square with a spacing of 8 cm between lamp centers. This source provided more even illumination over the 12 cm x 16 cm field and an optional water filter (1 cm of H_2O) was also provided for use with these lamps in order to filter out some of the unwanted infrared radiation. (3) Source No. 3 consisted of the xenon lamp in a PRA model ALH 200 water cooled housing. The output of this lamp passed through an optional water filter (6 cm of H_2O) and an optional glass filter to further remove near IR radiation. The output beam was expanded and collimated to provide a final output beam which was fairly uniform (± 10%) over a 16 x 16 cm field and had a divergence half angle of 4° or less. The xenon lamp was powered by a PRA model M301 DC power supply. This power supply provides a modulation input whereby an AC signal could be applied to provide varying degrees of AC modulation in the DC output of the lamp. This AC signal was supplied by a PAR model 124 lock-in amplifier.

The total radiant energy incident on a test surface was measured in the early experiments with a Coherent Radiation model 210 power meter and later an Epply Thermopile detector model No. E6 with an absolute calibration of ± 2% was used.

In a few experiments a 5 mW He/Ne laser was used to provide a monochromatic source. The output beam of the laser was expanded with a simple two-lens beam expander to provide an irradiance of approximately 100 mW/cm^2 (close to that of AM1 sunlight).

The electrical power output from the PEC was measured by recording the voltage drop across a 0.5 Ω resistor and across the total load which included a variable resistor in series with the PEC and the 0.5 Ω resistor. The power output could then be measured as a function of load resistance. During certain tests in which the xenon light source was partially modulated the AC component of PEC output was measured using the tuned amplifier portion of the PAR model 124 lock-in amplifier, which also provided the modulation signal. In a few tests the phase delay between the light source modulation and the PEC output was also measured using the phase sensitive amplifier of the lock-in. A Hewlett-Packard 6224B power supply was used to charge the storage electrode which was subsequently discharged into a variable resistor network. The internal cell resistance was measured with a Hewlett-Packard 4328A milliohmmeter.

A Hg/HgO (1M NaOH) reference electrode was used to measure the potentials of the photoelectrode and counter electrode both in the dark and under illumination.

A brief description of cells A, B and C will be given here and the reader is referred to ref. 1 and 2 for a more detailed description. In cell B the photoconversion electrode and the counter electrode were arranged side-by-side. The latter consisted of a small carbon strip, 3 mm wide and 14 cm long, placed between neighboring photoelectrodes which were 5 x 2 cm. The cell contained 10 photoelectrodes and was 13 cm wide by 11 cm high. The photoelectrodes were arranged with their long dimension vertical and in 5

vertical columns each containing 2 electrodes.

Cell A had the same number of photoelectrodes as cell B but they were arranged in two vertical columns, 5 to a column, with the long side of the photoelectrode horizontal. Each of the 6 counter electrodes were 15 mm x 125 mm and were placed in the cell perpendicular to the photoelectrode. Both cells contained storage compartments separated from the counter and photoelectrodes by a "Nafion" cation exchange membrane. The storage electrode was a silver/silver sulphide couple. The storage electrodes for both cell A and B were fabricated in the following manner. Silver powder of 100 mesh and 44 micron maximum size was pressure sintered onto both sides of a silver sheet measuring 10 cm x 17 cm x 0.2 cm. The sintered sheets were divided into individual electrodes measuring 10 cm x 2 cm with a total surface area of 40 cm^2. The storage capacity was approximately 20 mAh/cm^2. The design of cell A incorporated 6 electrodes having a combined storage capacity of approximately 4.8 Ah. Cell B was constructed with 5 storage electrodes mounted on a lucite plate. This arrangement limited the surface area to one side of an electrode therefore the storage capacity of cell B was approximately 2 Ah.

Cell C which was designed for maximum flexibility comprised of twelve 5 x 2 cm photoelectrodes each in individual cells, 4 of which also contained storage electrodes.

The photoelectrode was 2 mm from the cell window and two graphite counter electrodes (1.9 x 5 cm) were positioned at right angles to, and on either side of the photoelectrode. The total counter electrode area is 19 cm^2. The storage electrode, which was fabricated as for cells A and B, was 1.9 x 4.8 cm with a total surface area of 18.2 cm^2.

RESULTS

EVALUATION OF PHOTOELECTROCHEMICAL CELLS A AND B

PHOTOCONVERSION EFFICIENCY

The photoconversion efficiency of cell A was evaluated using source No. 1 (one single tungsten filament lamp). The lamp was set-up 38 cm from the cell to give an intensity of 92.5 mW/cm^2 (using the Coherent Radiation power meter). This intensity was arbitrarily chosen to define a standard condition which was close to AM1 conditions in total radiant intensity. The spectral output of the lamp was measured some months later when the calibration

source became available. The results of this calibration are shown in Figure 2. Since the spectral curve does not approximate AM1 sunlight it is not possible to express the light output in terms of a sunlight equivalent. The curve in Figure 2 was integrated from 300 nm to 730 nm and the resulting total radiation in this band-pass was 45 mW/cm^2. Thus of the total incident radiation of 92.5 mW/cm^2, 45 mW/cm^2 was capable of producing electrons in the CdSe.

The results are shown in Figure 3, 4 and 5 where the photovoltage and the power produced is shown versus photocurrent. In Figure 3 the results for the total photocurrent with all the photoelectrodes in parallel is shown, while Figure 4 and 5 show similar results for individual photoelectrodes. When an individual photoelectrode was tested that electrode was positioned on the axis of the light source in the region of maximum intensity. However, since the radiation intensity was non-uniform over the large area of the PEC, not all of the electrodes received the same illumination during the test of all the electrodes in parallel. Figures 4 and 5 show results for a poor and a good photoelectrode, respectively. Table I lists the open-circuit voltages, short-circuit currents and maximum electrical power produced for each of the photoelectrodes. A little over 1% of incident radiation in the 300-730 nm wavelength region is converted into electrical power by the best of the photoelectrodes.

In Figure 6 results for cell B (all photoelectrodes in parallel) are shown and the data on individual photoelectrodes is given in Table II. From the results in Tables I and II it can be seen that the electrical power produced with all the photoelectrodes in parallel is considerably less (approximately 3 x less) than the sum of the powers of the individual photoelectrodes. At least in part that can be attributed to the non-uniform intensity distribution of source No. 1 over the large areas of the total photoelectrode surface.

A similar series of tests was later carried out with source No. 2 (the bank of 4 tungsten filament lamps) equipped with a water filter. As for source No. 1, source No. 2 was later calibrated and the results are shown in Figure 7. The total intensity, as measured by the Coherent Radiation power meter, was 92.5 mW/cm^2 as before. The integrated intensity from 300 to 730 nm, obtained from integrating the data used in Figure 7, is 59 mW/cm^2. Since the lamps used in source No. 2 were identical to that used in source No. 1, the different integrated intensities found for the two sources in the 300-730 nm region is no doubt due to the use of the water filter which removed much of the IR radiation. (The total intensity, as measured by the power meter, was of course the same for both sources).

The power and voltage curves as a function of photocurrent are shown in Figure 8 and 9 for cells A and B, respectively. The data on individual photoelectrodes are presented in Table III and IV. The data in Table IV show that the best of the individual electrodes for cell B are converting approximately 0.5% of the incident radiation in the 300 to 730 nm region into electrical power. For cell A the corresponding figure is 1.7%. The total output of each cell is considerably greater than for single lamp illumination. This undoubtedly reflects the more uniform illumination. However, the sum of the powers produced by individual photoelectrodes is still

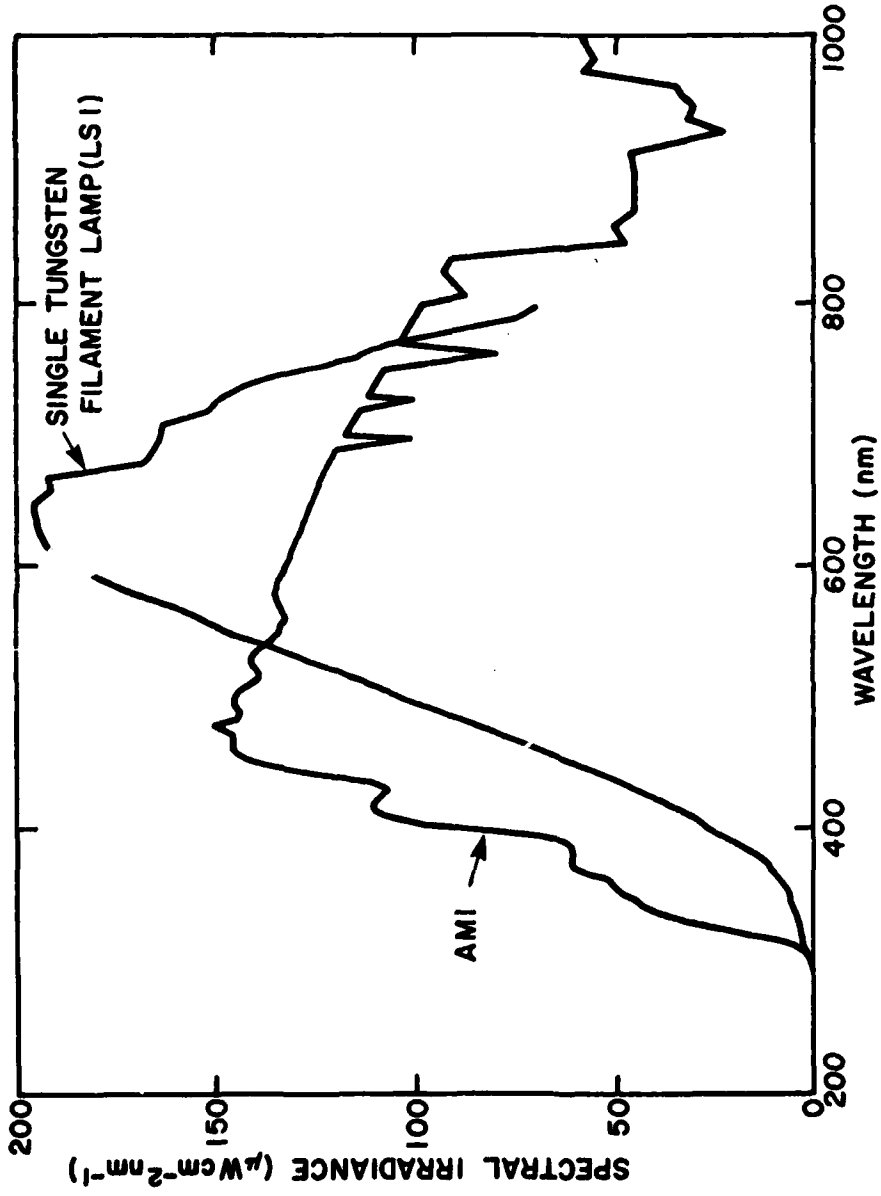

Fig. 2: Calibrated spectral irradiance for a single tungsten filament lamp, Light Source 1, with AM1 standard shown for comparison.

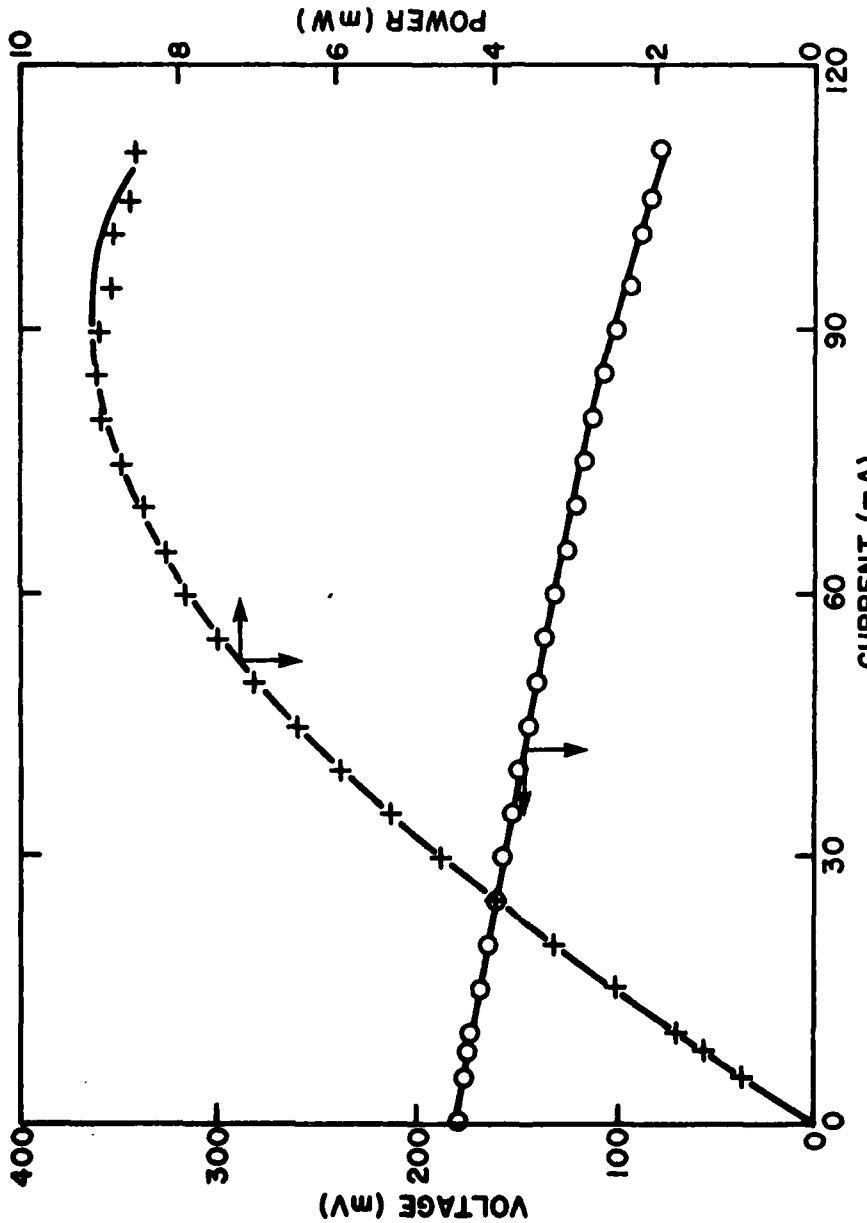

Fig. 3: Electrical performance of Cell A (Irradiated by Light Source 1).

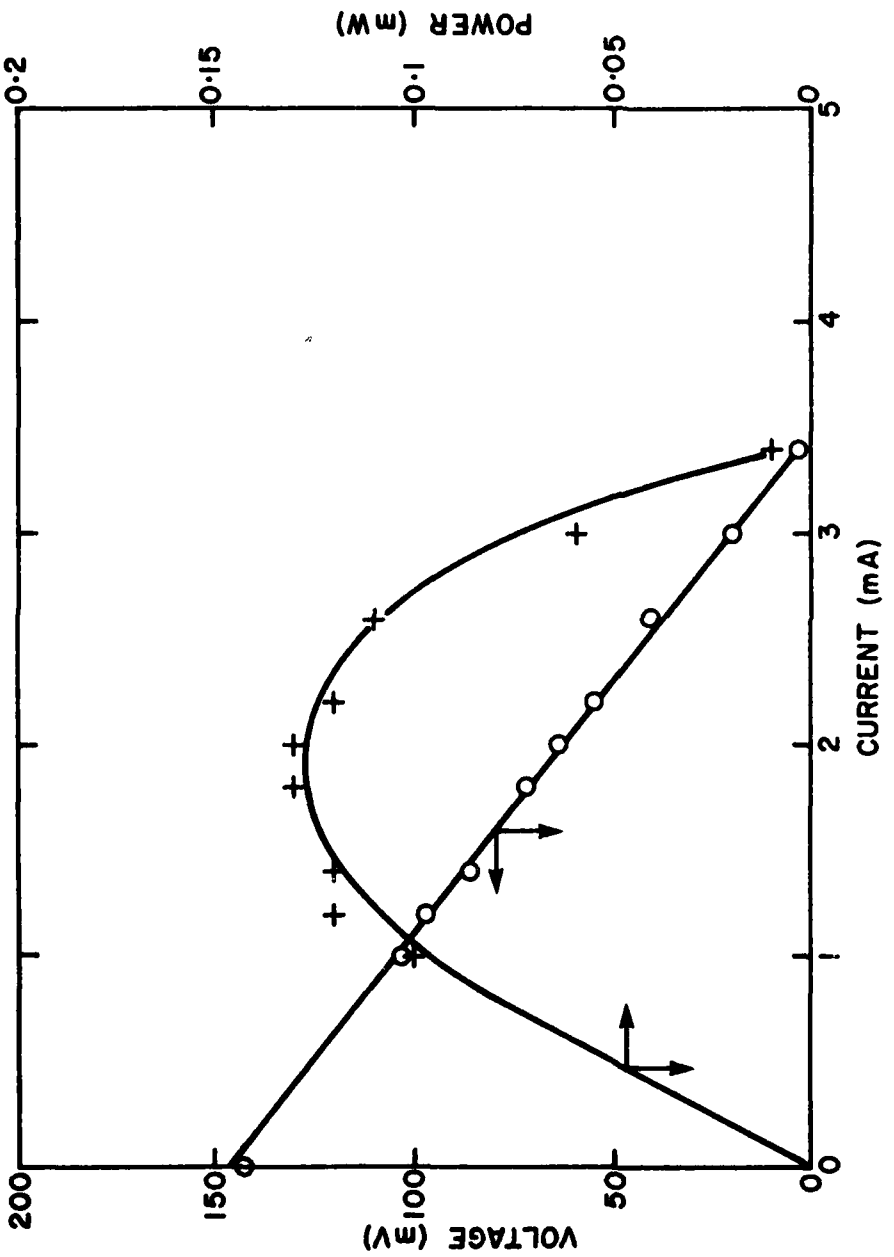

Fig. 4: Electrical performance of photoelectrode 2, Cell A. (Irradiated by region of maximum intensity of Light Source 1).

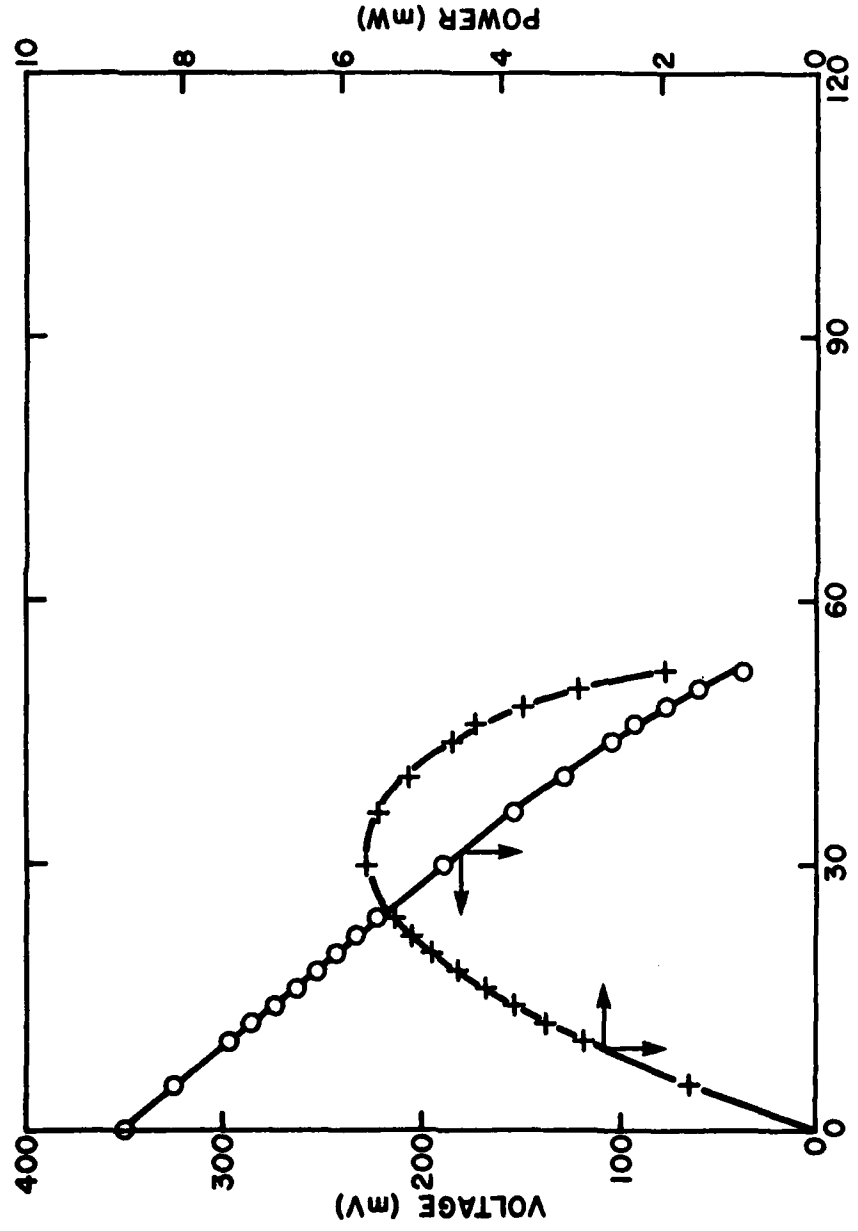

Fig. 5: Electrical performance of photoelectrode 10, Cell A. (Irradiated by region of maximum intensity of Light Source 1).

TABLE I

Electrical Performance of Cell A
(Irradiated by Light Source 1)

Photoelectrode	Open-Circuit Voltage (mV)	Short-Circuit Current (mA)	Maximum Electrical Power (mW)
All*	179.0	110.6	9.0
1	155.0	24.0	1.3
2	143.0	3.4	0.1
3	263.1	59.1	5.1
4	305.4	46.2	5.4
5	271.8	28.0	2.1
6	146.0	30.0	1.5
7	174.3	36.1	2.4
8	185.1	32.4	2.0
9	196.4	28.6	1.8
10	360.0	52.0	5.7

* The single tungsten-filament lamp did not illuminate all the photoelectrodes uniformily. Individual photoelectrodes were positioned so that the electrode was in the region of maximum intensity.

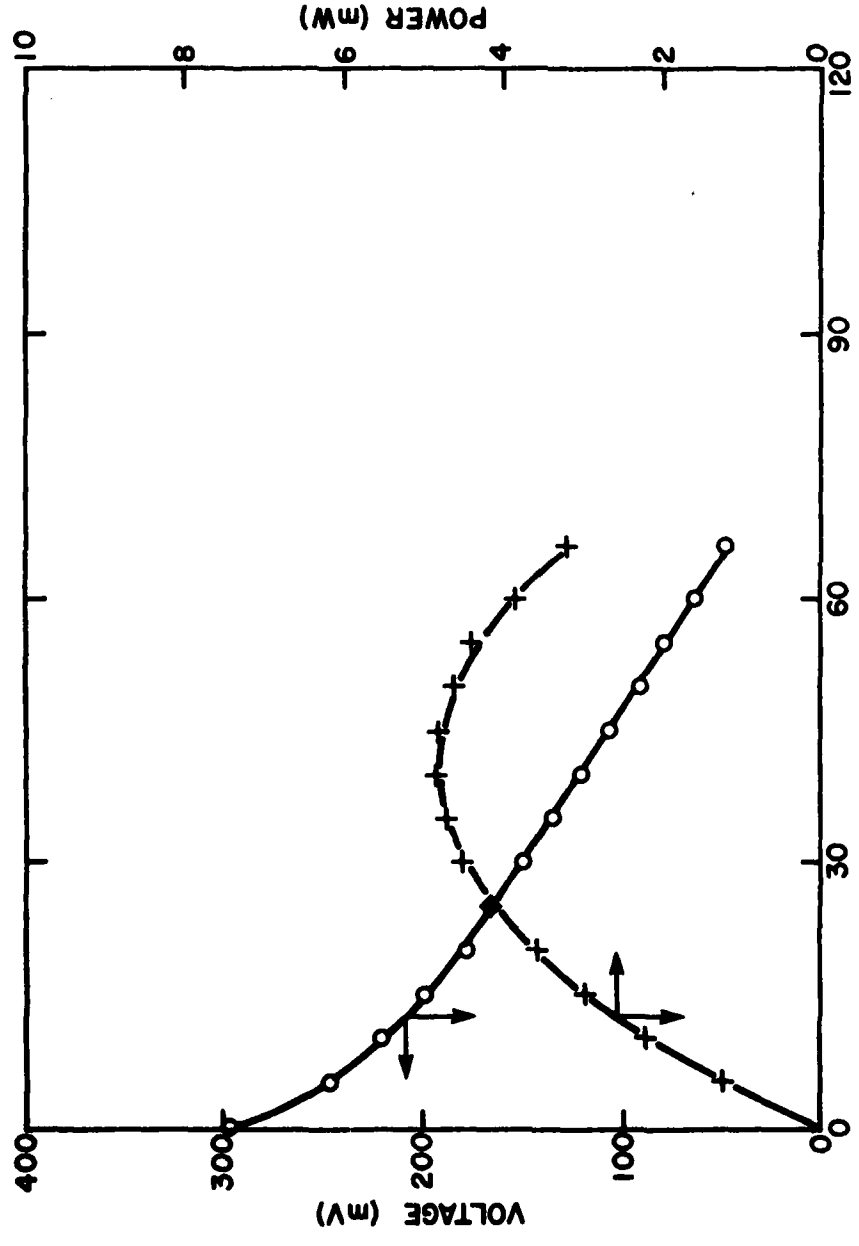

Fig. 6: Electrical performance of Cell B. (Irradiated by Light Source 1).

TABLE II

Electrical Performance of Cell B
(Irradiated by Light Source 1)

Photoelectrode	Open-Circuit Voltage (mV)	Short-Circuit Current (mA)	Maximum Electrical Power (mW)
All[a]	297.1	66.0	4.8
1	378.3	25.1	2.6
2	315.0	26.3	2.6
3	224.4	11.0	0.7
4	33.0	-	-
5[b]	320.8	24.6	2.0
6	345.9	21.9	2.3
7	299.3	22.1	2.2
8	216.0	16.4	1.0
9[c]	-	-	-
10	338.6	32.3	3.2

a The single tungsten-filament lamp did not illuminate all the photoelectrodes uniformly. Individual photoelectrodes were positioned so that the electrode was in the region of maximum intensity.

b,c Electrodes with broken electrical contacts.

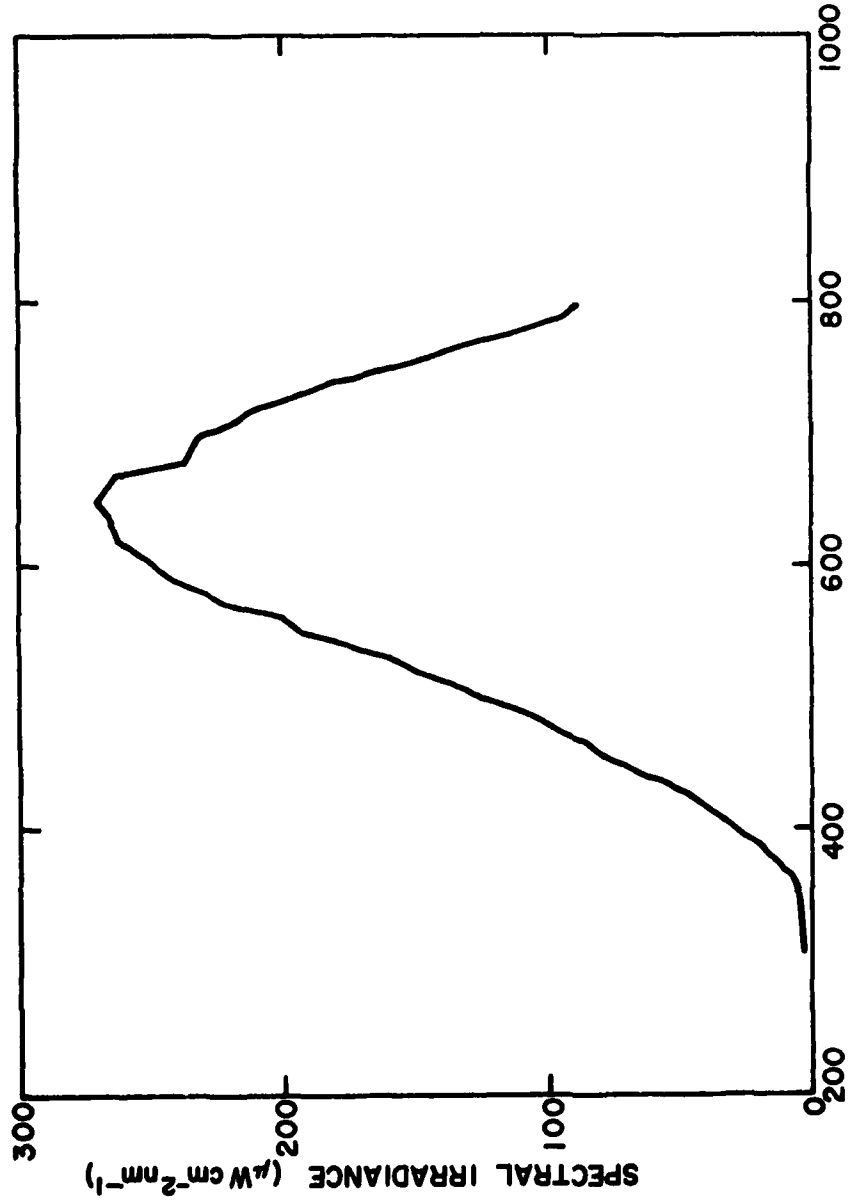

Fig. 7: Calibrated spectral irradiance for the bank of 4 tungsten filament lamps, Light Source 2.

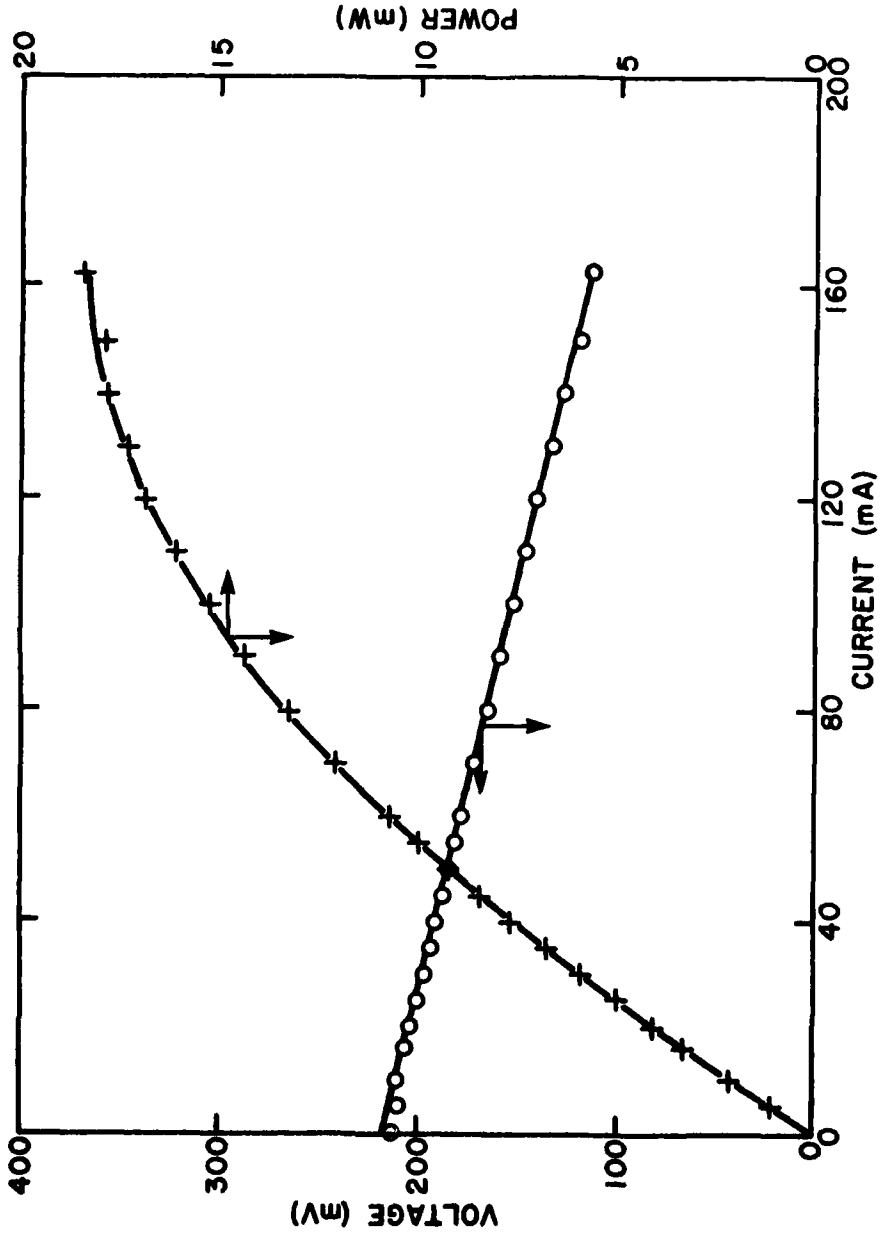

Fig. 8: Electrical performance of Cell A. (Irradiated by Light Source 2).

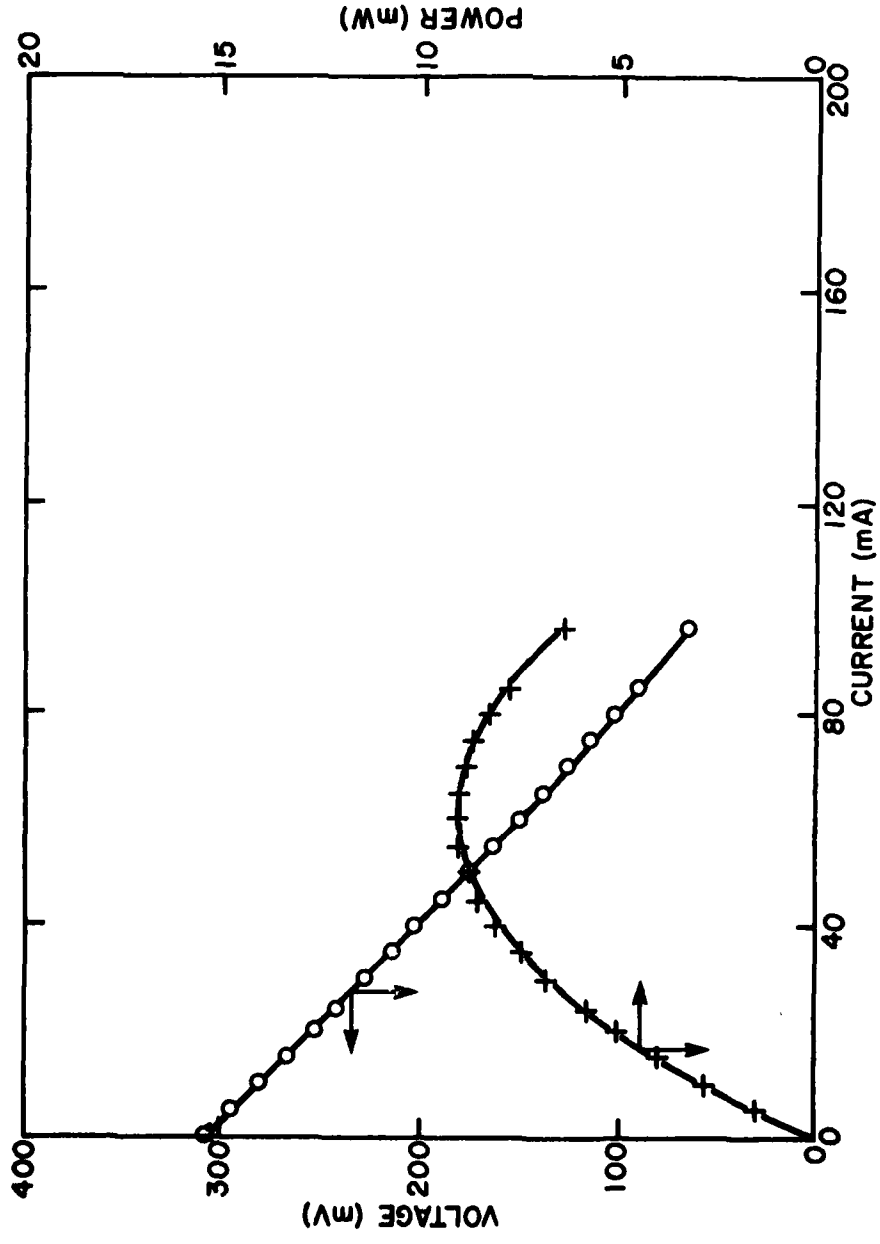

Fig. 9: Electrical performance of Cell B. (Irradiated by Light Source 2).

TABLE III

Electrical Performance of Cell A
(Irradiated by Light Source 2)

Photoelectrode	Open-Circuit Voltage (mV)	Short-Circuit Current (mA)	Maximum Electrical Power (mW)
All	213.6	163.4	18.4
1	103.3	29.1	1.0
2	154.9	9.8	0.4
3	176.0	70.6	4.6
4	336.1	88.0	11.0
5	243.3	50.4	3.8
6[a]	-	-	-
7	169.5	68.2	4.1
8[b]	-	-	-
9	200.7	4.0	0.2
10	322.0	95.1	10.0

a,b Electrodes with broken electrical contacts.

TABLE IV

Electrical Performance of Cell B
(Irradiated by Light Source 2)

Photoelectrode	Open-Circuit Voltage (mV)	Short-Circuit Current (mA)	Maximum Electrical Power (mW)
All	308.5	96.2	9.1
1	338.1	25.6	2.7
2	319.9	28.0	2.4
3	280.0	9.0	0.7
4	227.3	0.6	0.0
5	322.8	19.0	1.8
6	350.1	24.0	2.3
7	285.6	28.4	2.3
8	254.9	16.7	1.3
9	120.4	0.2	0.0
10	337.0	29.9	2.7

larger (approximately twice) than the total power observed with all the photoelectrodes in parallel.

A third series of tests was carried out with the xenon lamp (source No. 3-1) when it became available. The calibration of this source with a Schott tempax 112F glass filter is shown in Figure 10 along with the curve for AM1 sunlight. The overall intensity of the light source was adjusted to give the best match to AM1 sunlight in the 300-730 nm range. The integrated intensity of the xenon source in this wavelength range was 48.9 mW/cm^2; for comparison, the standard AM1 curve shown in Figure 10 gives 46.6 mW/cm^2 in this wavelength interval and 88.9 mW/cm^2 over the complete wavelength range 290 to 4045 nm. Thus our xenon source (No. 3-1) is approximately equivalent to an AM1 source of intensity (48.9/46.6) x 88.9 mW/cm^2 or 93.3 mW/cm^2. This latter number can now be used for estimating an overall solar conversion efficiency. We have endeavoured to match the AM1 spectral distribution in the 300-730 nm region as closely as possible. However, the absolute intensity of our source in this wavelength interval is sometimes as much as 15% different to the AM1 intensity. Rather than find, by trial and error, a position in the beam which exactly matches this AM1 intensity we have normalized all our measurements to AM1 intensity as described above.

The results obtained with cell A and using the xenon light source are shown in Figure 11 and Table V. It can be seen from the results that the performance of the cell had deteriorated in that only one photoelectrode (No. 10) was operating at reasonable efficiency. This electrode was converting 0.6% of the light in the 300-730 nm range to electrical power. Based on the equivalent AM1 source of 93.3 mW/cm^2 given above this efficiency is 0.33%. This is the efficiency for conversion of AM1 sunlight to electrical power. The total power obtained from all photoelectrodes is now, to a good approximation, equal to the sum of the powers of the individual photoelectrodes. This probably results from the more uniform illumination (± 10% over total field of source No. 3-1).

ELECTRODE POTENTIAL MEASUREMENTS

During the course of this test program the performance of the PEC's deteriorated. This was particularly true of cell B. This cell developed a permanent open-circuit potential even under non-illuminated conditions. In order to trace the origin of this effect measurements were made of electrode potentials against the Hg/HgO reference electrode described earlier.

For cell A, which was not demonstrating the permanent polarization, the counter electrode and photoelectrode voltages were 612 and 616 mV, respectively under dark conditions. The difference in these two values corresponds to the 0-5 mV dark potential which a normally functioning cell developed under open-circuit conditions. On illumination with the xenon source (at approximately AM1 conditions) the potential of the various photoelectrodes increased to 678-898 mV while the counter electrode remained constant at 612 mV. Thus as expected the open-circuit potential developed by the PEC resulted from an increase in potential of the photoelectrode.

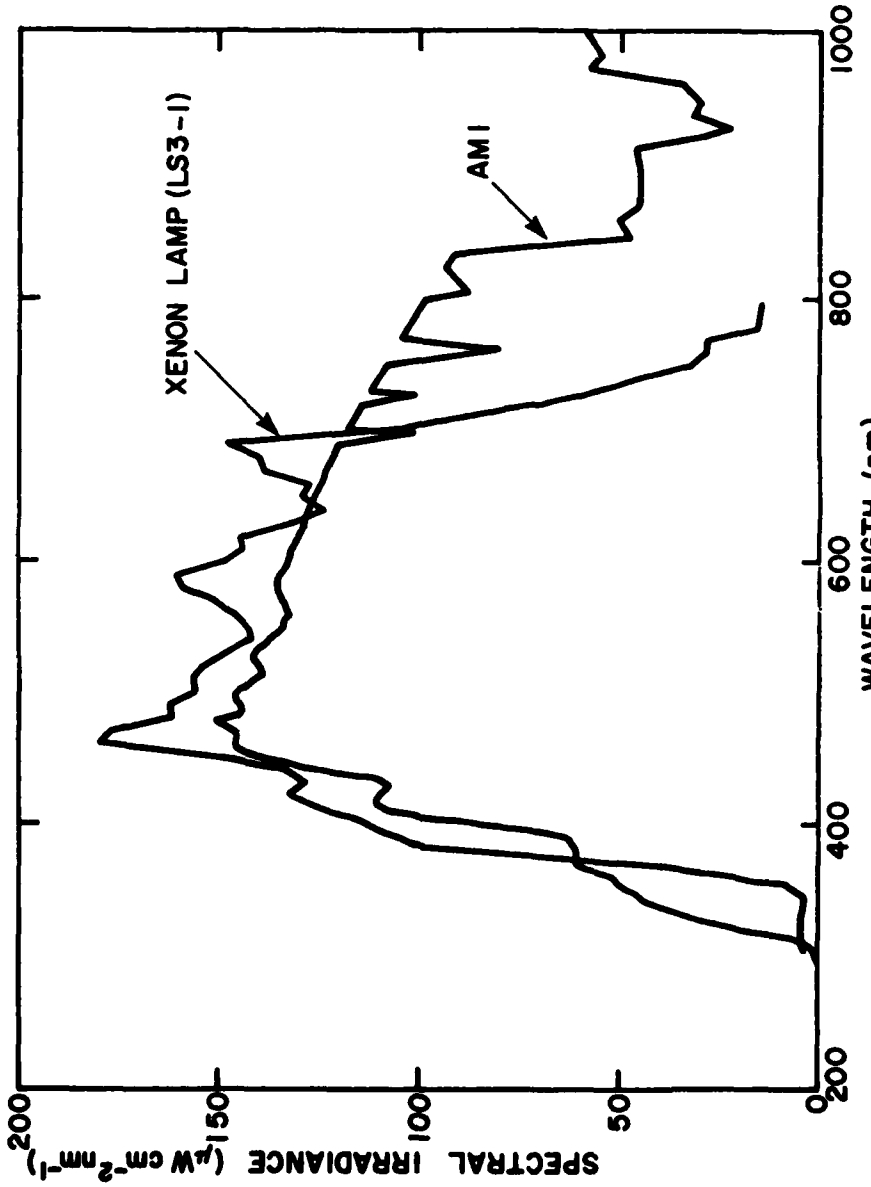

Fig. 10: Calibrated spectral irradiance for Xenon lamp, Light Source 3-1, with AM1 standard shown for comparison.

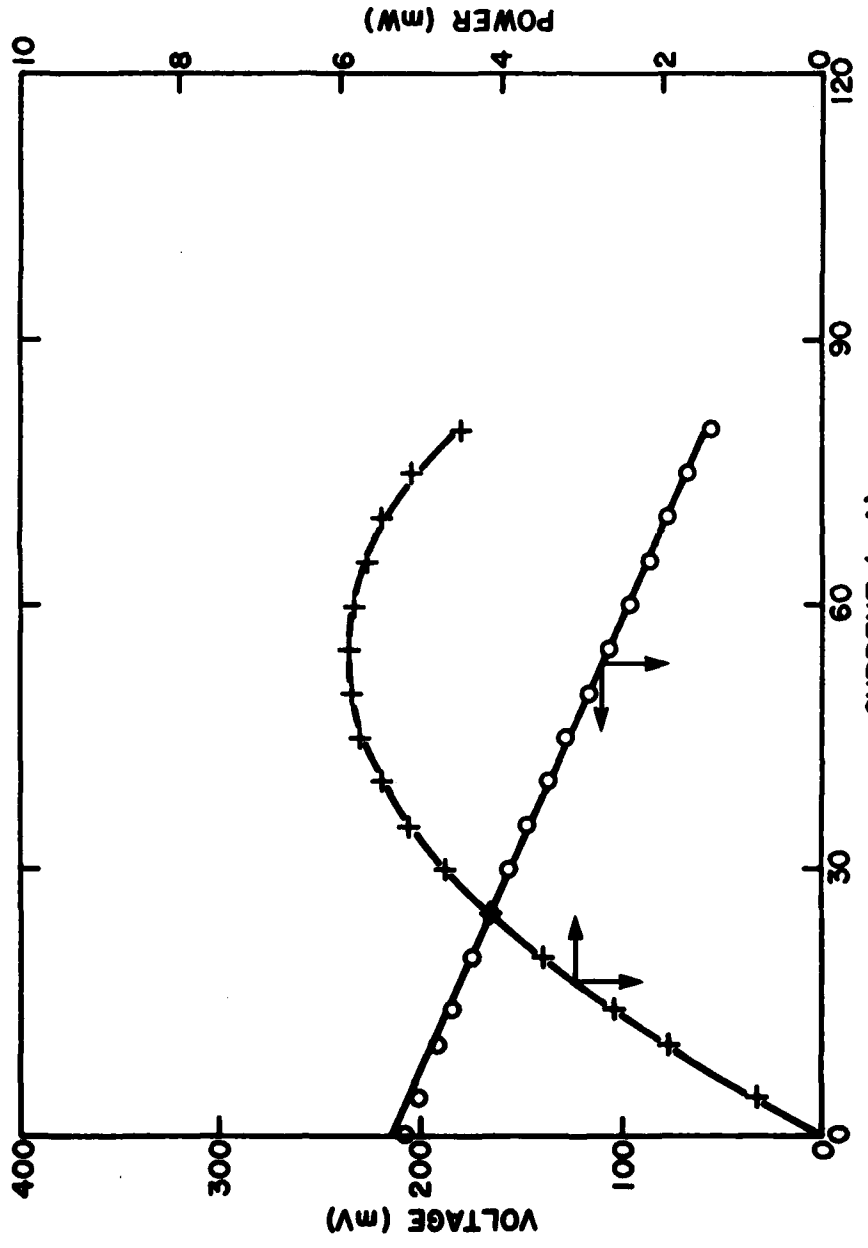

Fig. 11: Electrical performance of Cell A. (Irradiated by Light Source 3-1).

TABLE V

Electrical Performance of Cell A
(Irradiated by Light Source 3-1)

Photoelectrode	Open-Circuit Voltage (mV)	Short-Circuit Current (mA)	Maximum Electrical Power (mW)
All	208.0	80.4	5.9
1[a]	-	-	-
2[b]	-	-	-
3	200.9	12.3	0.8
4	148.7	9.3	0.3
5	198.7	15.8	0.8
6[c]	-	-	-
7	142.1	26.6	1.13
8[d]	-	-	-
9[e]	-	-	-
10	269.1	37.0	3.1

a,b,c,d,e Electrodes with broken electrical contacts.

For cell B, however, the dark photoelectrode potentials fell in the range 290 to 592 mV, although the counter electrode potential remained at 612 mV, identical to that of cell A. Thus the negative photoelectrode potentials which were externally observed are caused by a drop in the potential of the photoelectrode. These differences in absolute potential between the photoelectrodes and the counter electrodes corresponded to those observed externally. On illumination the counter electrode potential remained essentially constant (614 mV) whilst the various photoelectrode potentials measured from 440 to 756 mV. Thus, as with cell A, the photoelectrode potential increased on illumination. The measurements demonstrated that the dark potential observed in cell B was attributable to a change in the potential of the photoelectrode.

IN SITU ENERGY STORAGE

The evaluation of the in situ storage was accomplished by cycling the storage electrodes while monitoring the charge capacity and power utilization. Initial attempts to charge the storage electrodes with the power produced by the photoelectrodes failed. The photoelectrode potentials developed under AM1 illumination resulted in charging levels less than 1 mA. At such low current levels thousands of hours of continuous charging would be required to fully charge the storage electrodes. In order to characterize the conditions required to charge the storage electrodes tests were conducted with an external power supply connected between the counter electrode and storage electrodes. The results for a series of discharge/charge cycles for each PEC are shown in Table VI while typical profiles are seen in Figures 12 and 13.

The nominal open-circuit voltage for a charged storage compartment of cell A was 155 to 165 mV. This cell was discharged at various current levels in the range of 20 to 90 mA and delivered between 3.5 and 4.4 Ah or 0.22 and 0.30 Wh. Constant current charging at 100 and 200 mA resulted in a charge acceptance of 4.1 Ah. The discharge to charge power ratio was approximately 0.2. Open-circuit voltages ranging from 220 to 230 mV were recorded for cell B. The storage capacity was approximately 2.3 Ah while maintaining discharge levels between 15 and 50 mA and the charge acceptance was approximately 2 Ah for charge rates of 50 and 100 mA. The discharge to charge power ratio of cell B was less than 0.1. The reason for the inefficient charging of the storage electrodes by the photoelectrodes becomes evident when the required charging potential (300 to 900 mV) is compared to the nominal open-circuit voltage (200 mV) developed by the photoelectrodes under AM1 illumination.

Various other observations were made during the evaluation of the in situ storage capability of PEC's. The internal resistance between the storage electrodes and the counter electrodes was 250-500 mΩ for cell A and 800 to 1200 mΩ for cell B. During the final stage of a charging cycle, a yellow precipitate (possibly sulfur) was deposited on the storage electrodes. This was more noticeable in cell A where 50-70% of the storage electrode surface area was covered. The deposit disappears quickly on a discharge cycle.

TABLE VI

Charge/Discharge Characteristics of In Situ Storage Compartments for Photoelectrochemical Cells A and B

	DISCHARGE							CHARGE					
	Voltage (mV)		Current (μA)		Duration	Capacity		Voltage (mV)		Current	Duration	Capacity	
	I	F	I	F	(hrs)	(mAhr)	(mWhr)	I	F	(mA)	(hrs)	(mAhr)	(mWhr)
CELL A	154	59	20	40	114	4059	257						
								340	376	201	20.67	4113	1519
	169	38	92	43	79.67	4403	219						
								419*	283	101	41.33	4133	1359
	155	66	48	30	94.67	3495	295						
CELL B	220	38	26	15	137.67	2319	101						
								431	859	103	20	2039	1164
	231	14	46	20	90.33	2314	43						
								389	517	50	43.33	2149	934

I = Initial

F = Final

* Artificially high due to loose connection

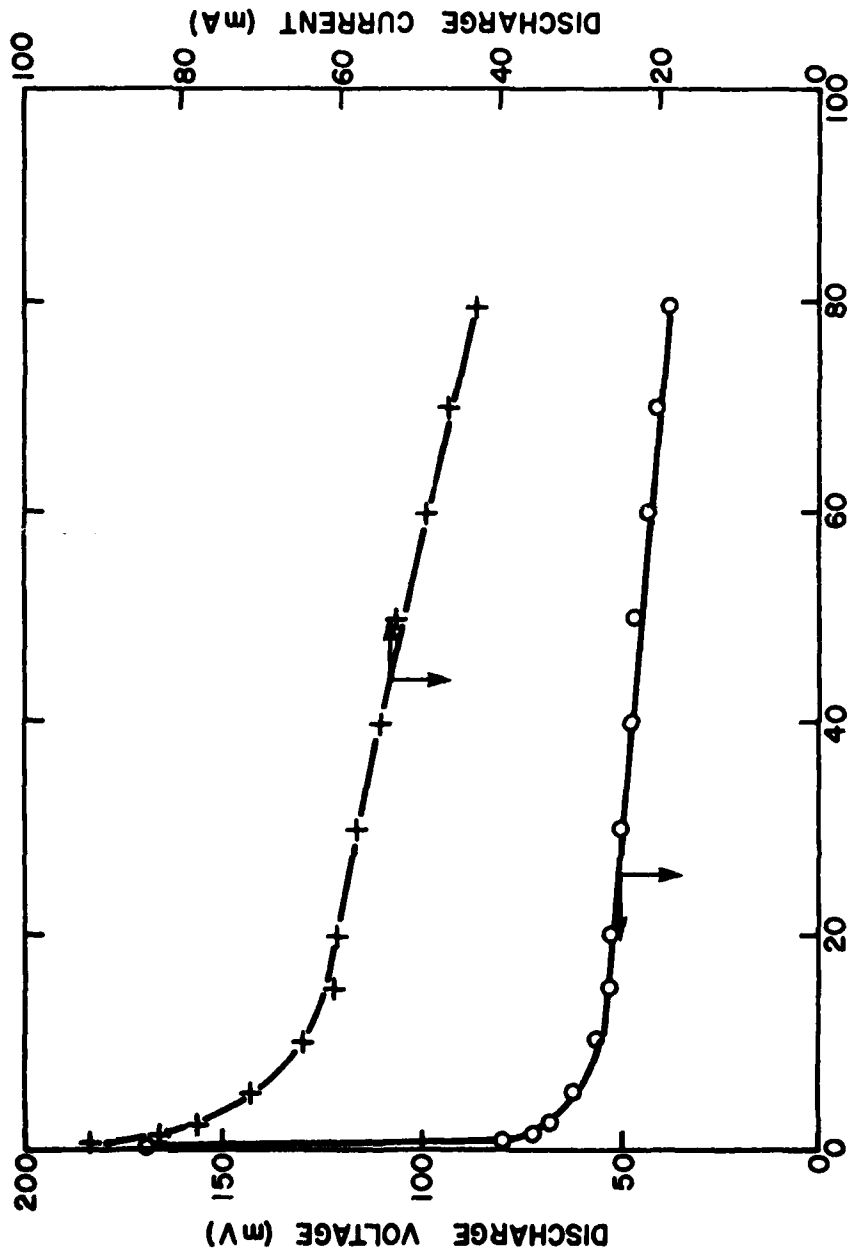

Fig. 12: Typical discharge profile for storage compartment of photoelectrochemical cell A.

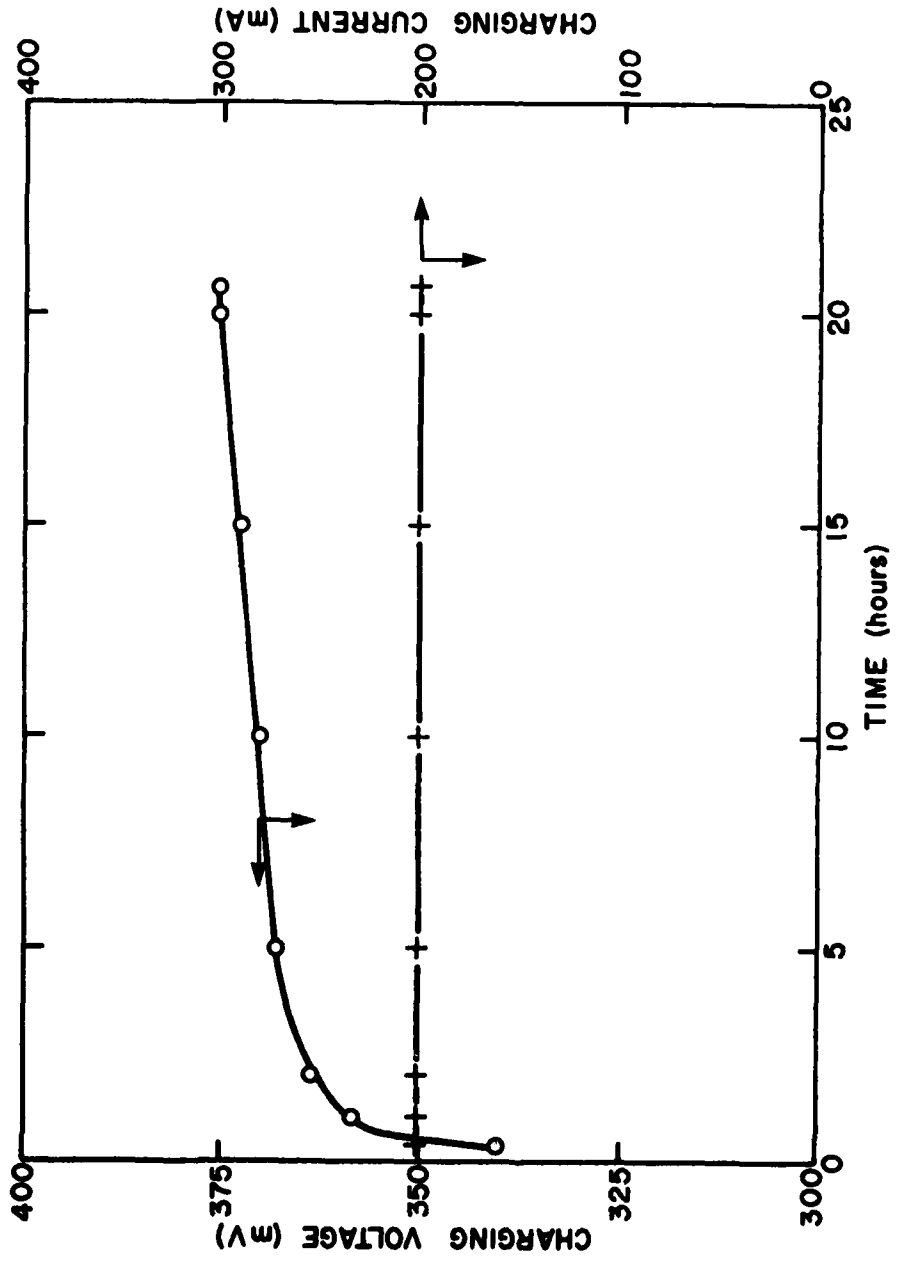

Fig. 13: Typical charge profile for storage compartment of photoelectrochemical cell A.

Finally, an osmotic process appears to have caused electrolyte loss in cell A. During discharge cycles, electrolyte tends to bleed through the filler-port located on the counter electrode side of the Nafion membrane. This is probably caused by water migration across the Nafion membrane to keep the sulphide ion concentration equal. During discharge, sulphide ions are consumed in the storage compartment to form Ag_2S. The electrolyte loss amounts to 10-20 milliliters over a period of 75-100 hours.

EVALUATION OF SERIES C PHOTOELECTROCHEMICAL CELLS

PHOTOCONVERSION EFFICIENCY

The photoconversion efficiency of Series C PEC's was determined with the xenon lamp (source No. 3-2) which had a spectral distribution closer to that of AM1 sunlight than the source used for the evaluation of Cell A (Figure 9). This was accomplished by removing the Schott filter and using a 6 cm water filter. The match to our AM1 reference was extended 75 nm, from 750 to 825 nm. Once again the overall intensity of the lamp was adjusted to closely match AM1 sunlight in the 300-730 nm wavelength range, resulting in an intensity of 50.3 mW/cm^2 in this band which is equivalent to a source with AM1 spectral distribution and a total irradiance of 96.1 mW/cm^2. The calibration can be seen in Figure 14.

The typical electrical performance of the Series C PEC's is shown in Table VII. It should be remembered that Series C was comprised of 12 individual cells; 8 cells with a 10 cm^2 photoelectrode and 20 cm^2 of carbon counter electrode (referred to as cells 1 through 8) and 4 cells with the above specifications plus a storage compartment (referred to as cells 9 through 12). Of the 12 cells received, only 6 cells were capable of producing better than 0.5 mW of power and, interestingly, four of these were storage cells. The maximum power output recorded was 1.4 mW with Cell 9. The short-circuit currents observed ranged from a low of 2 mA (Cell 8) to a high of 22 mA (Cell 10) - a maximum current density of 2.2 mA/cm^2. The open-circuit voltages varied between 200 and 350 mV the average of the 12 cells being 297 mV. The best polarization and power curve recorded for this series, with Cell 9, is shown in Figure 15.

The solar to electrical conversion efficiencies can be calculated using the data presented in Table VII and the lamp calibration. Once again, two efficiencies were calculated - one based upon radiant intensity at wavelengths below the band-gap of the device (300-730 nm), the other based upon a total equivalent terrestrial AM1 intensity. The irradiation level simulated by the xenon lamp in the band-gap region was 50.3 mW/cm^2 while the equivalent terrestrial AM1 intensity was 96.1 mW/cm^2. The two efficiencies as well as a fill-factor (refer to discussion for definition) were calculated for each of the 6 best cells of Series C, the results presented in Table VIII.

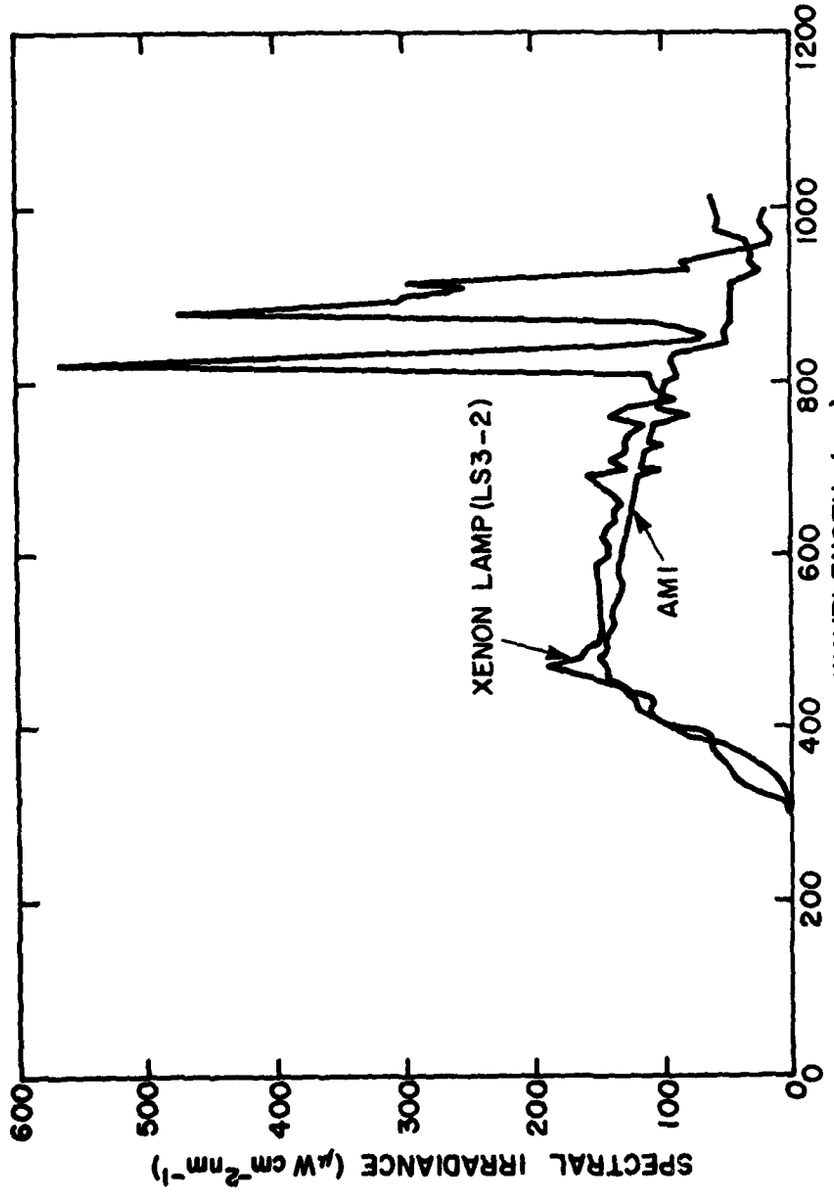

Fig. 14: Calibrated spectral irradiance for Xenon lamp, Light Source 3-2, with AMI standard shown for comparison.

TABLE VII

Electrical Performance of Series C Cells
(Irradiated by Light Source 3-2)

Photoelectrode	Open-Circuit Voltage (mV)	Short-Circuit Current (mA)	Maximum Electrical Power (mW)
1	295	7	<0.5
2	294	6	<0.5
3	270	3	<0.5
4	338	18	0.76
5	298	8	0.49
6	300	4	<0.5
7	313	5	<0.5
8	200	2	<0.5
9	350	20	1.40
10	322	22	0.89
11	287	12	0.63
12	293	10	0.62

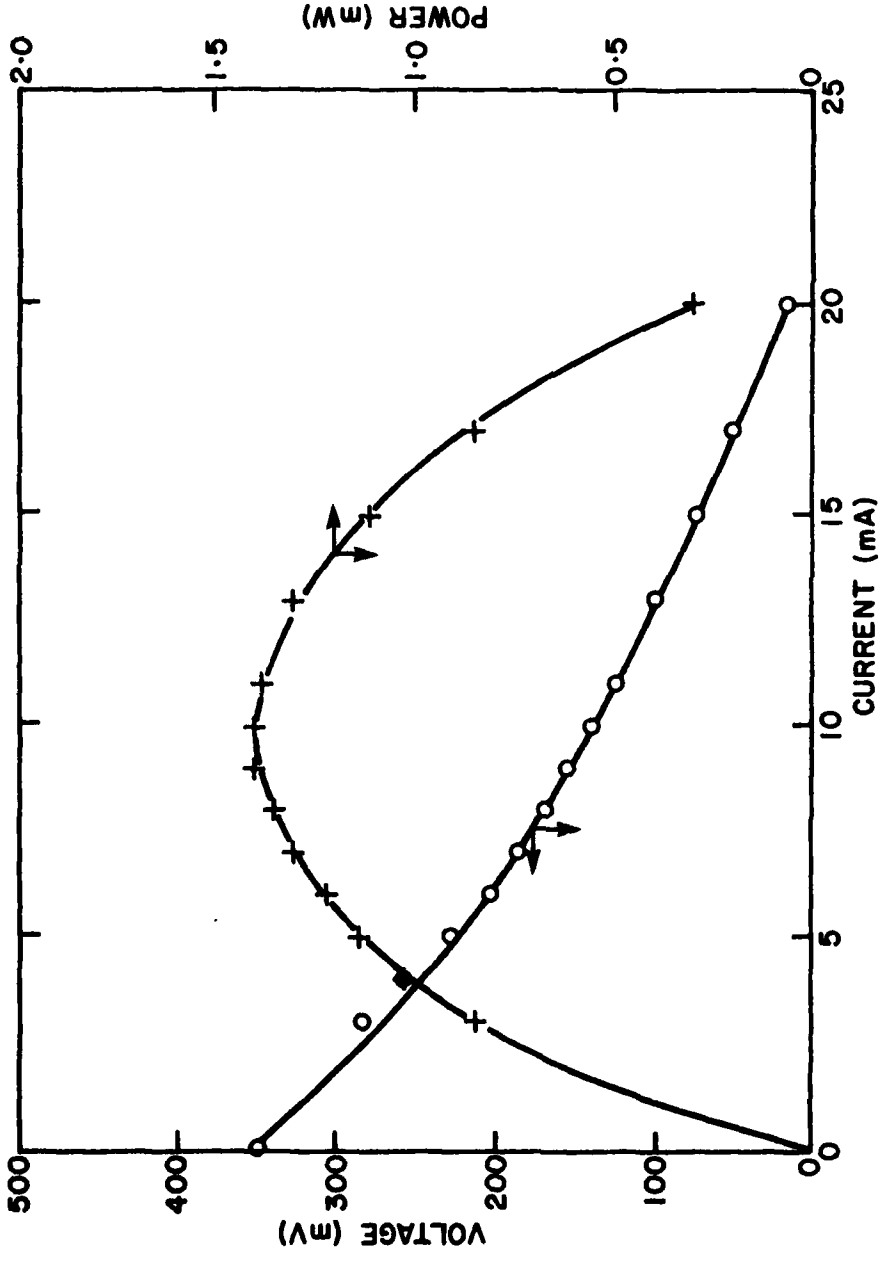

Fig. 15: Electrical performance of Cell 9, Series C Cells. (Irradiated by Light Source 3-2).

TABLE VIII

Fill-Factor and Efficiency Calculations for Selected Photoelectrochemical Cells of Series C

Photoelectrode	Fill-Factor	Efficiency (300-730 nm) (%)	Efficiency (AM1 Equivalent) (%)
4	0.13	0.15	0.08
5	0.21	0.10	0.05
9	0.20	0.28	0.15
10	0.13	0.18	0.09
11	0.18	0.12	0.06
12	0.21	0.12	0.06

The highest conversion efficiency of radiation in the 300-730 nm band was 0.28% for Cell 9. This cell had an open-circuit potential of 350 mV, a short-circuit current of 20 mA and produced a maximum power of 1.4 mW. The overall solar to electrical conversion efficiency for Cell 9 was 0.15%.

During the course of the evaluation it was observed that the maximum power output of some cells did not deteriorate as a function of time but in fact the maximum power output increased. An example of this can be seen in Figures 16 and 17. Figure 16 shows 3 polarization curves obtained with Cell 4 over a period of two months while the corresponding power curves appear in Figure 17. The data recorded for Cell 4 on March 5 was as follows: open-circuit voltage - 338 mV, short-circuit current - 18 mA, maximum power output - 0.76 mW. On March 28, under similar conditions and the same electrolyte the performance was: open-circuit voltage - 307 mV, short-circuit current - 10.5 mA, maximum power output - 0.85 mW. Even though the short-circuit current dropped significantly, 18 to 10.5 mA, the maximum power output increased from 0.76 to 0.85 mW. On April 30 this cell was re-examined and displayed the initial open-circuit voltage - 337 mV, a somewhat higher short-circuit current than the previous test, 12.4 mA compared to 10.5 mA, but the lowest power output to date - 0.57 mW. These results suggest that some cells undergo an initial conditioning period during which power output increases followed by a period in which the performance deteriorates.

ELECTRODE POTENTIAL MEASUREMENTS

Polarization characteristics of the carbon counter electrodes and the cadmium selenide photoelectrodes were determined by measuring their potentials against a Hg/HgO reference electrode. Similar measurements were presented for PEC's A and B when reporting on the permanent open-circuit potentials observed under dark conditions. The individual electrode potential measurements for Cells 4 and 12 are presented schematically in Figure 18. An open-circuit potential of 615 to 620 mV appears at the counter electrode under dark conditions. The dark potential of the photoelectrode is normally within 10 mV of the counter electrode, the difference corresponding to the observed dark potential of the cell. As expected, under illumination and open-circuit conditions, the counter electrode potential remains constant and the potential at the photoelectrode increases. The photoelectrode potentials for Cells 4 and 12 increased 206 and 310 mV respectively, resulting in open-circuit cell potentials of 207 and 318 mV. However, as shown in Figure 18, under AM1 illumination and at maximum current demand (short-circuit conditions), voltage polarization at the counter electrode amounts to approximately 70% of the open-circuit cell potential. The counter electrode current density at which the above mentioned losses occurs was approximately 0.5 mA/cm^2 for Cell 4 and 0.36 mA/cm^2 for Cell 12. Significant counter electrode polarization (60%, 194/318 mV) was recorded with Cell 12 at a counter electrode current density of 0.06 mA/cm^2. The polarization characteristics of the electrodes are influenced by the magnitude of the light intensity as shown in Table IX. As the light intensity is reduced by introducing neutral density filters the polarization at the counter electrode decreases. For example, the data for Cell 12 in Table IX shows that under AM1 illumination

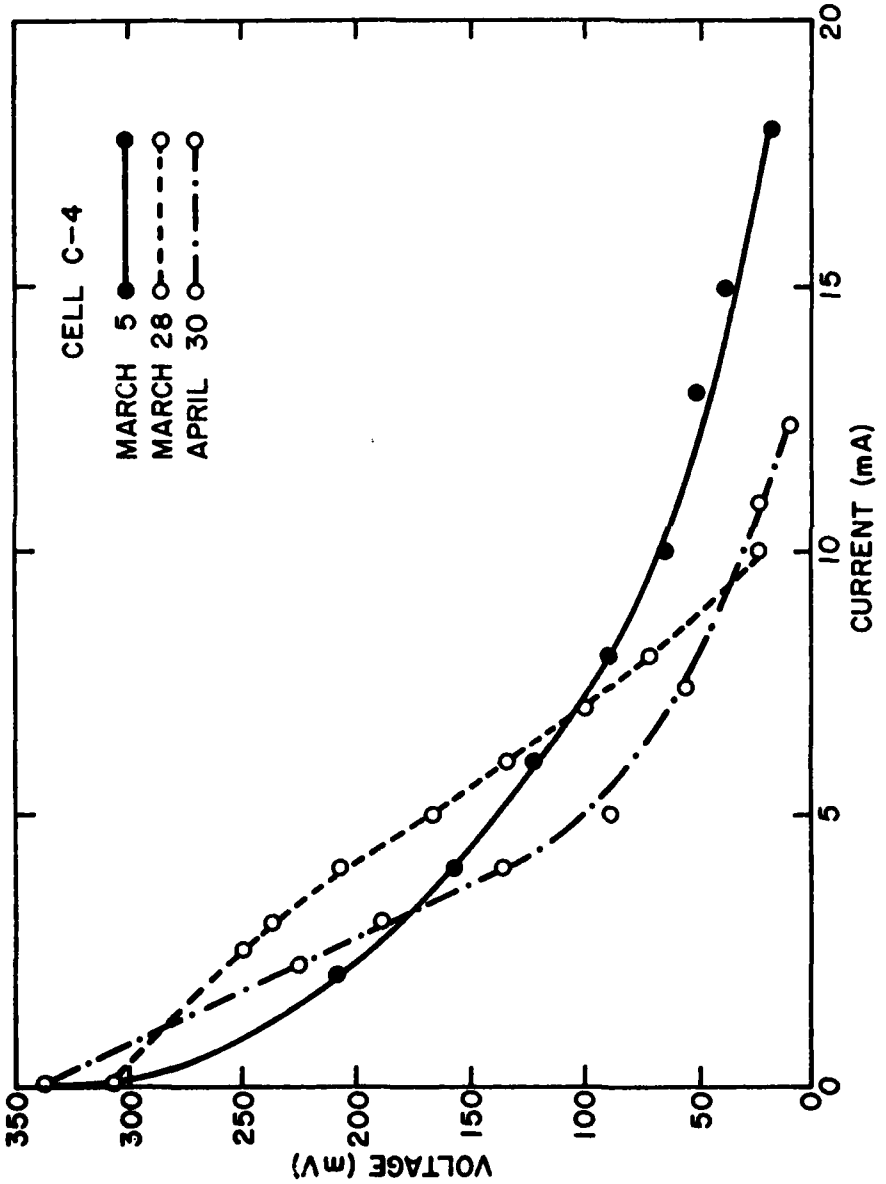

Fig. 16: Variation of the voltage-current characteristics of Cell 4, Series C Cells over an 8 week period.

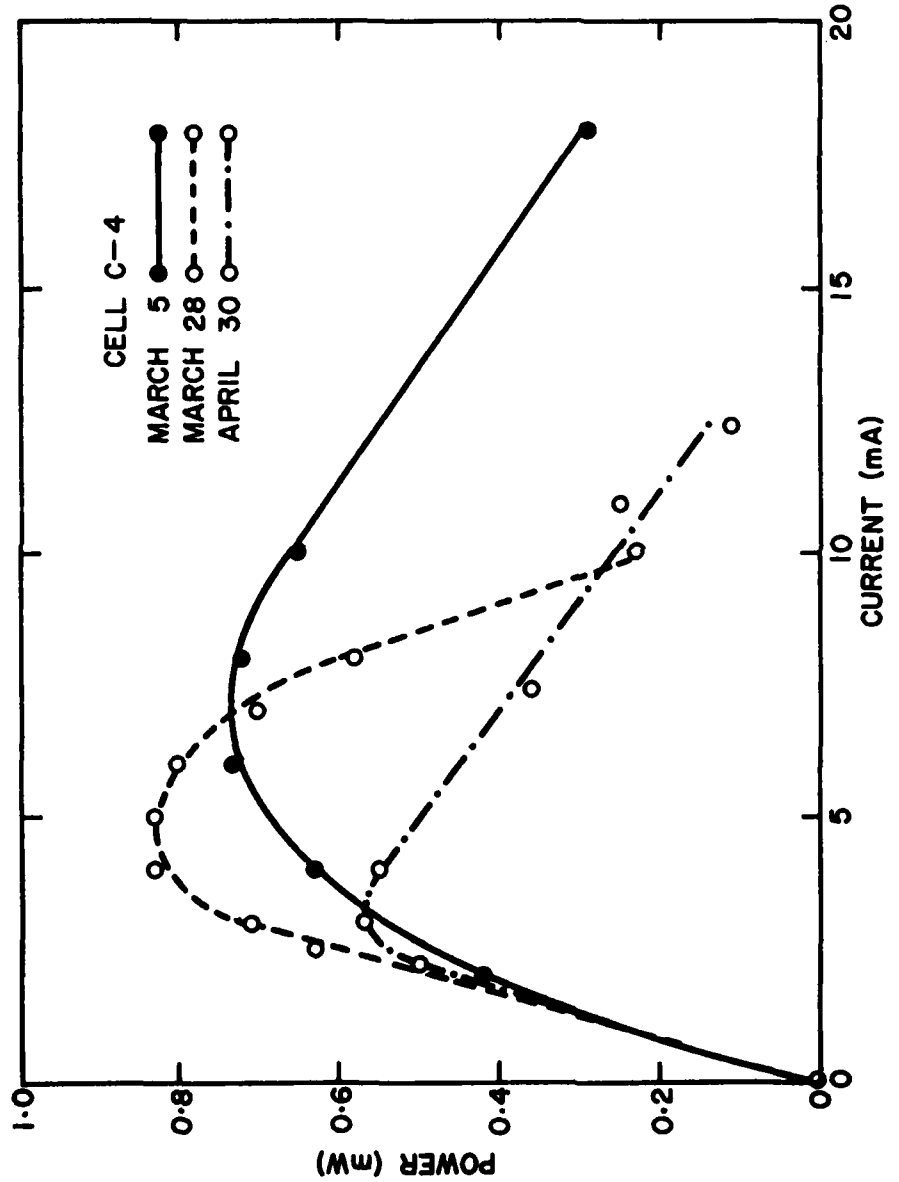

Fig. 17: Variation of the power output of Cell 4, Series C Cells over an 8 week period.

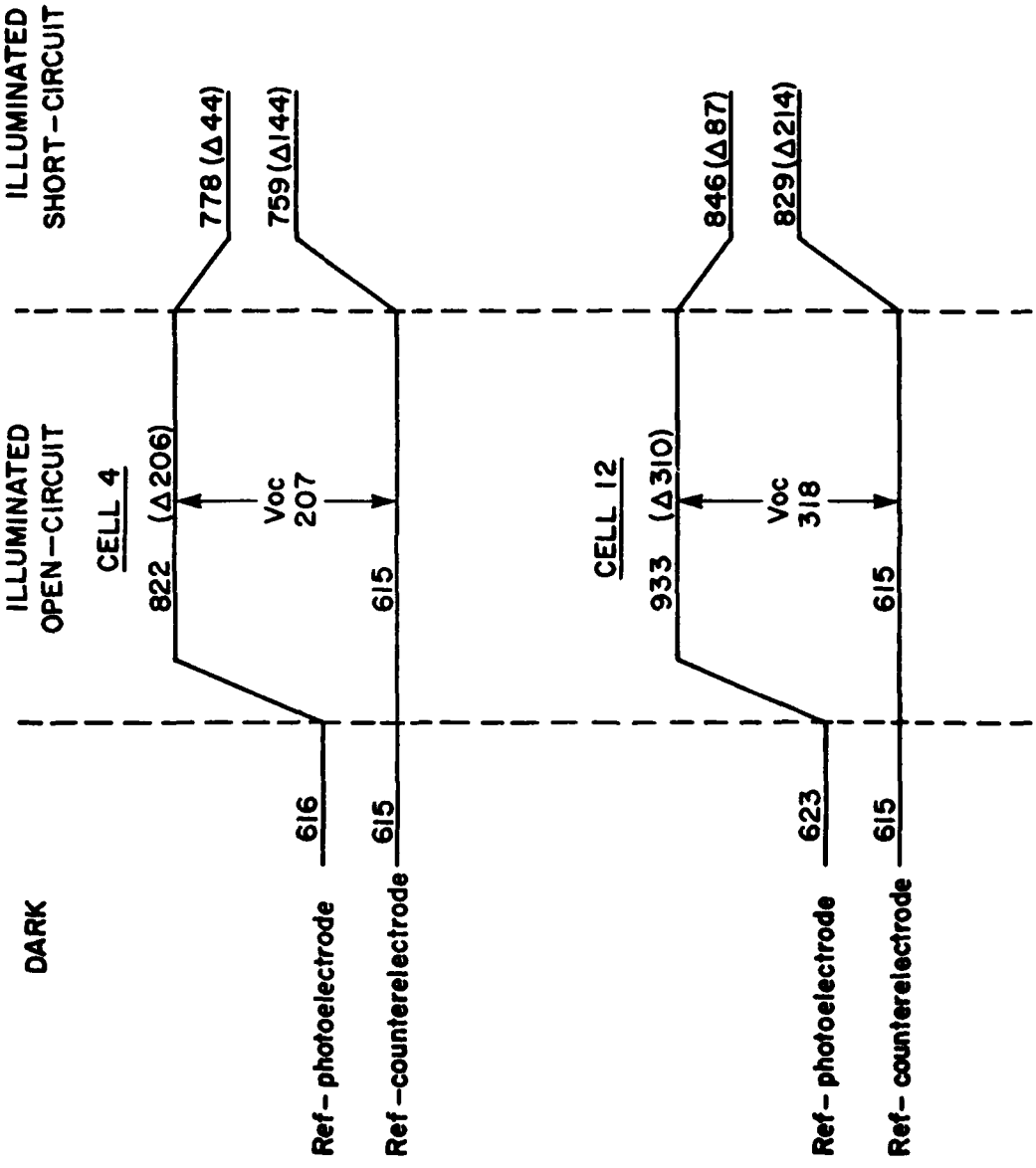

Fig. 18: Absolute potentials of the photoelectrode and counter electrode for cells 4 and 12, Series C Cells. (Hg/HgO as reference).

TABLE IX

Polarization Characteristics of the Photoelectrode and Counter Electrode as a Function of Light Intensity

Intensity Ratio	Open-Circuit Voltage (mV)	Short-Circuit Current (mA)	Counter Electrode[b] Polarization (mV)	Photoelectrode[c] Polarization (mV)
		Counter Electrode[a] Current Density (mA/cm^2)	% of Open-Circuit Voltage	% of Open-Circuit Voltage
1	318	7.2/0.36	214/67.3	82/27.4[d]
0.5	280	3.8/0.19	181/64.6	92/33.2
0.2	214	2.0/0.10	121/56.5	96/44.9
0.1	168	1.6/0.08	56/33.3	107/63.7

a Counter electrode surface area = 20 cm^2.

b,c Polarization at short-circuit current.

d Residual cell potential accounts for rest of open-circuit voltage.

(intensity ratio = 1) the polarization at the counter electrode amounts to 67% of the open-circuit cell voltage while at an intensity ratio of 0.1 the polarization is reduced to 33%. The corresponding polarization at the photoelectrode appears in Figure 19. The polarization is expressed as a percentage of the open-circuit cell voltage and is plotted against the intensity ratio.

Finally, the deterioration of the Series C cells has not paralleled the deterioration of photoelectrochemical Cell B in that the negative cell potentials recorded with Cell B have not been noticed with the Series C cells.

PHOTOELECTRODE SATURATION EFFECTS

The open-circuit voltage and the maximum obtainable electrical power were measured as function of light intensity. The results are shown in Figure 20 and 21. The light intensity was varied by interposing neutral density filters between the light source and the cell.

From Figure 20 it can be seen that the open-circuit voltage varies linearly with the logarithm of the light intensity for all of the cells investigated. The power output saturates with increasing light intensity for both cells 4 and 9 as shown in Figure 21. Thus these cells have a much higher photoconversion efficiency at reduced intensities. This represents a serious difficiency whose possible cause will be discussed later.

In order to determine the slope of plots such as those in Figure 21 the lamp output was modulated at a fixed frequency and both the AC and DC output currents of the cells were measured. It was anticipated that the AC response of the system would then give the variation in system performance about the DC operating point. The AC modulation was 3.2% RMS of the average DC level. The percentage modulation of the cell current as a function of average DC current is shown in Figure 22 for 3 different modulation frequencies. The observed modulation for a fully illuminated and partially illuminated (1 cm^2) electrode at a frequency of 150 Hz is shown in Figure 23. It is apparent that the modulation is dependent on the frequency and varies with the average current. A qualitative explanation for these effects will be given later but it is evident that the results cannot be simply interpreted to give the slopes of plots such as those in Figure 21.

HELIUM/NEON LASER PROBE MEASUREMENTS

The surface of several photoelectrodes were probed with a He/Ne laser in an attempt to disclose the location and possibly the cause of poor electrical performance. The laser provided a coherent light source which enabled the measurement of localized electrical performance, and thus, to determine if the poor electrical performance observed under AM1 illumination could be attributed to electrodeposition abnormalities.

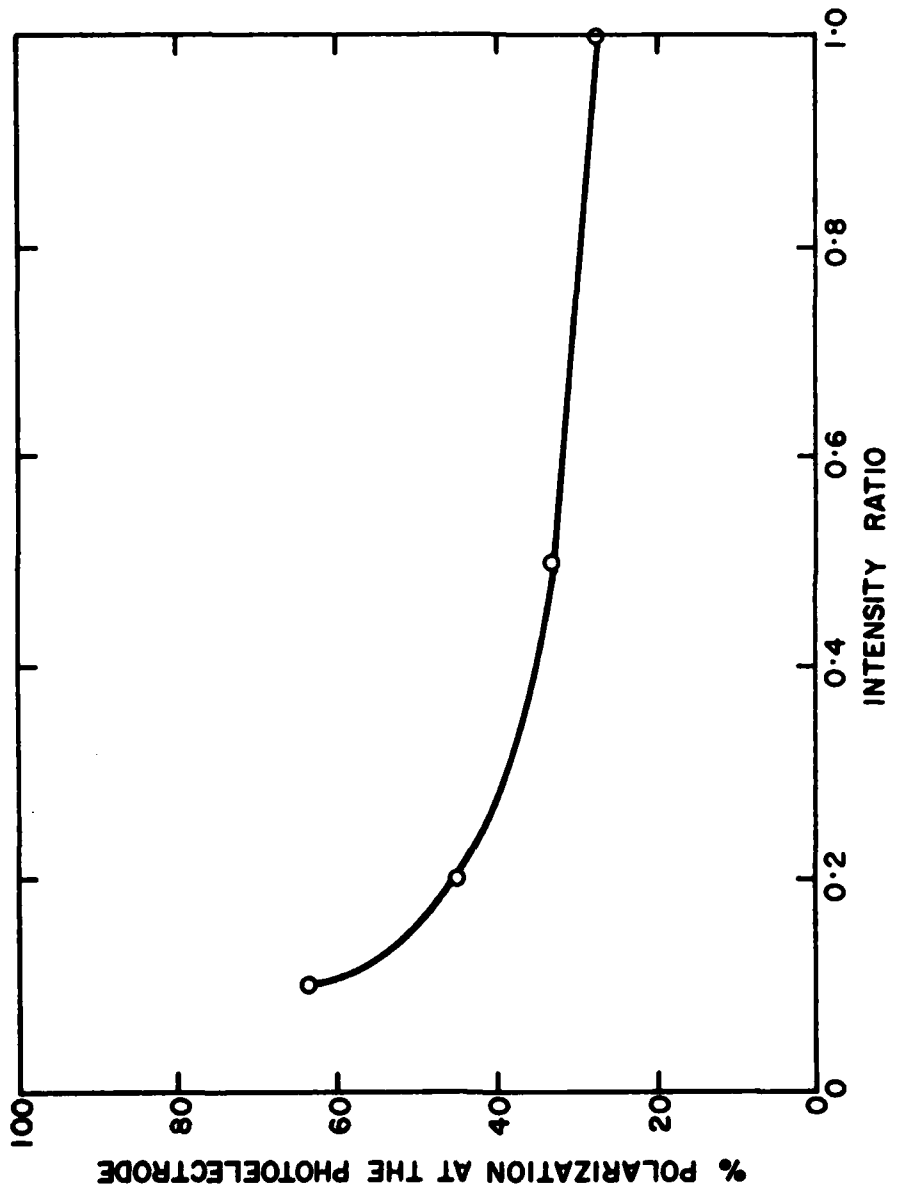

Fig. 19: Photoelectrode polarization as a function of light intensity. Expressed as a function of the open-circuit voltage.

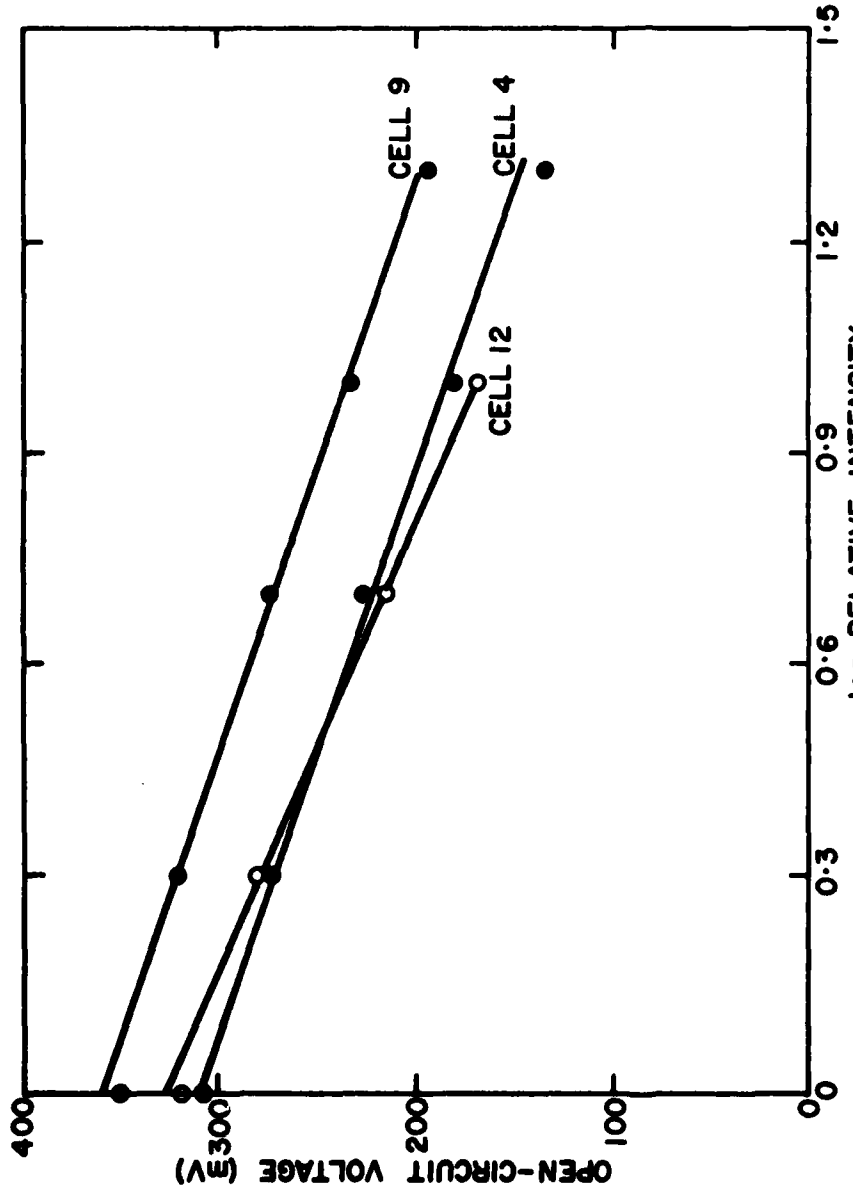

Fig. 20: Open-circuit voltage as a function of relative light intensity. An intensity of 1 corresponds to AMI illumination.

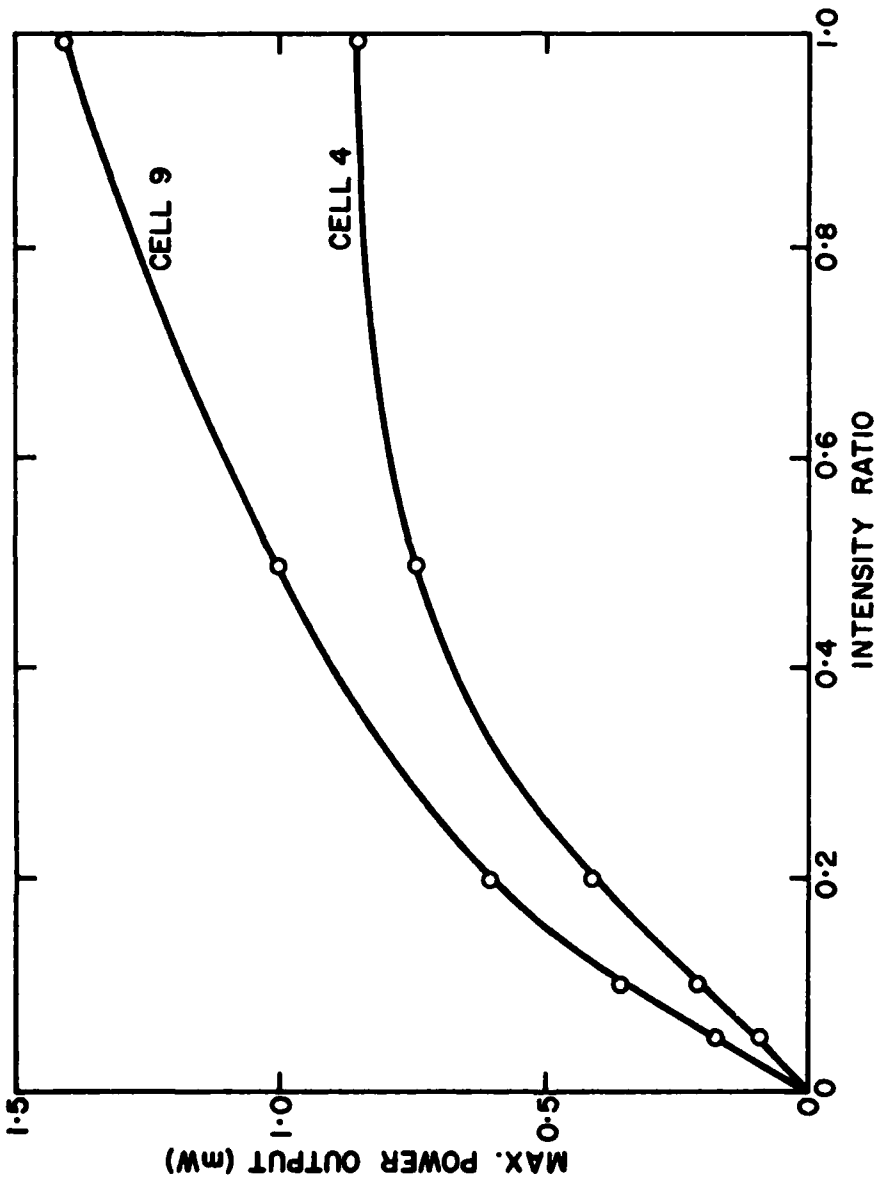

Fig. 21: Maximum power output as a function of relative light intensity.

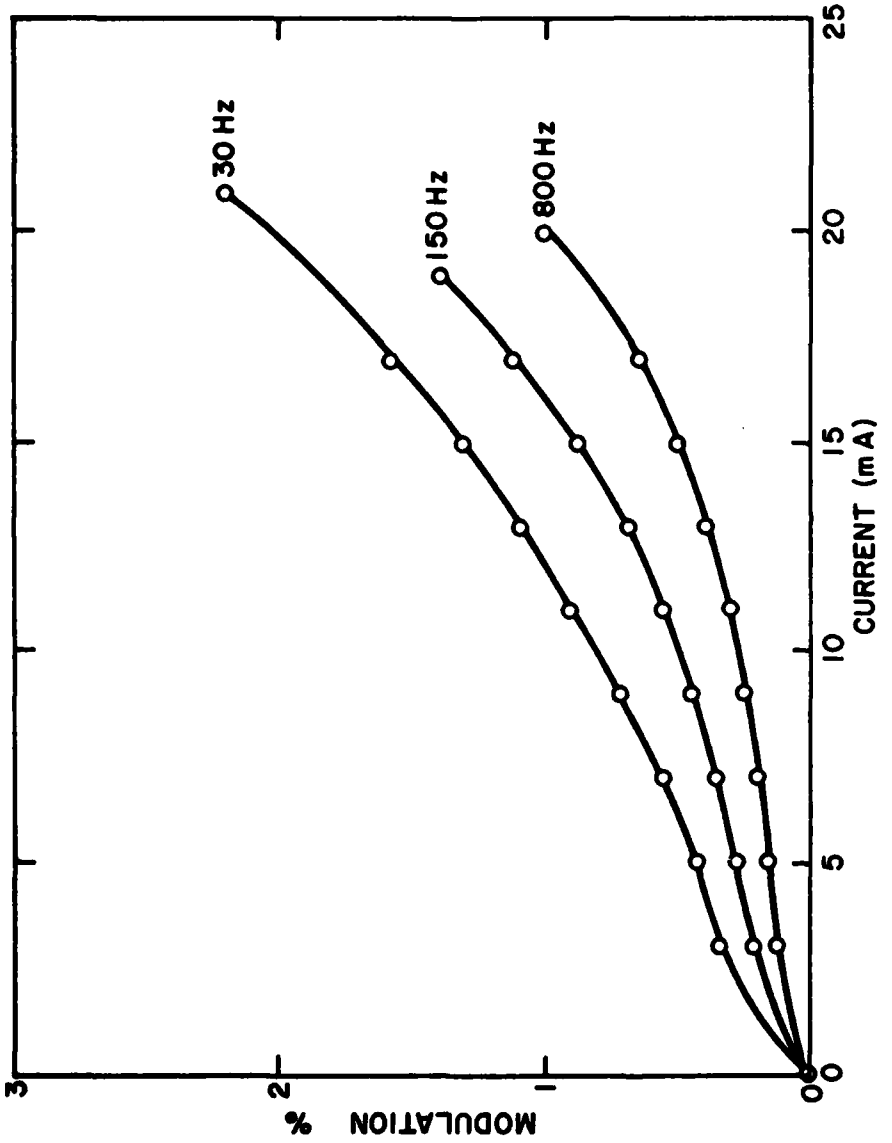

Fig. 22: Fractional current modulation as a function of modulation frequency. Modulation calculated as (AC component (RMS)/ Average DC current) x 100.

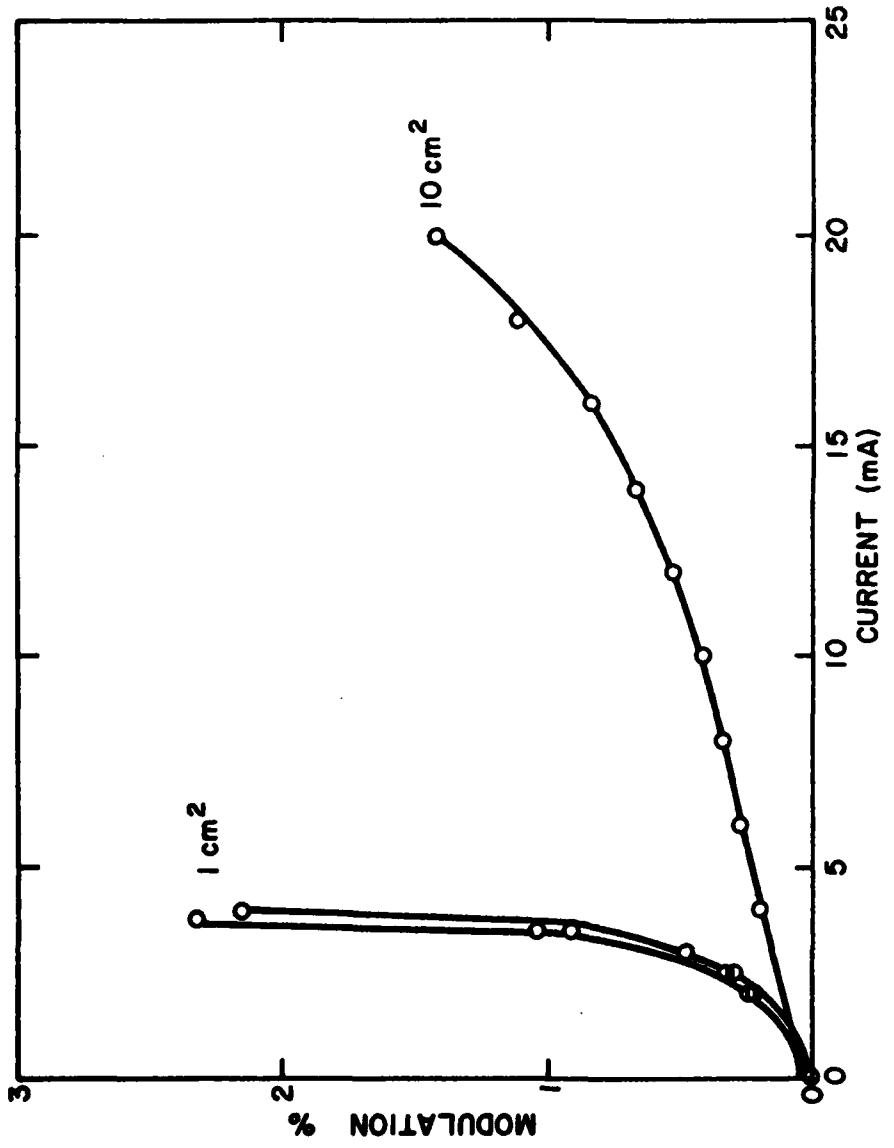

Fig. 23: Fractional current modulation for a fully illuminated (10 cm²) and a partially illuminated (1 cm²) electrode. The frequency used was 150 Hz and the two curves for 1 cm² illuminated area are for two different locations.

The monochromatic output beam (633 nm) of the laser was expanded to a diameter of 2.6 mm with a simple two-lens system providing an irradiance level of 78 mW/cm^2. A 3 x 5 matrix of localized electrical performance (open-circuit voltage and short-circuit current) was recorded for each photoelectrode examined. The absolute magnitude of the data is not significant but rather the relative response within a photoelectrode and between cells.

The laser probe results for 3 cells - 8, 9 and 10, are shown in Table X. Cell 8 was examined for two reasons, firstly, it was a cell that displayed poor electrical performance when received (open-circuit voltage of 200 mV and a short-circuit current of 2 mA) and secondly, a close visual examination of the photoelectrode revealed a partially discolored surface. The surface was a series of brown and black bands compared to a normal coloration of dark grey or black. This discoloration suggests a non-uniform electrodeposit. By comparison, Cells 9 and 10 demonstrated above average electrical performance (refer to Tables VII and VIII). The surface coloration of Cell 9 was similar to 8 - non-uniform, while the coloration of Cell 10 was homogeneous. The results show that the electrical response to the laser is directly related to the electrical performance under AM1 illumination, Cell 9 displaying the highest laser response and the best AM1 performance. The most interesting observation is the correlation between the surface coloration and the laser response. This can be seen clearly in the results for Cell 9 and to some degree with Cell 8, even though the overall response to the laser was poor for this cell. Referring to the results for Cell 9 in Table X, the following data points are important (the points are indexed to their vertical and horizontal position - VP, HP): VP-2, HP-2; VP-2, HP-3; VP-3, HP-3; VP-2, HP-4; VP-2, HP-5; VP-3, HP-5. The relative response of the above mentioned points are lower than neighboring laser responses and correspond to a discolored area of the photoelectrode. The same pattern can be seen to some degree in Cell 8 along the data points indexed as VP-1, HP-5; VP-2, HP-5; VP-3, HP-5. Once again these points correspond to an area of discoloration. For comparison, a uniform laser response was recorded for photoelectrode 10 which had a homogeneous coloration.

ELECTROLYTE ANALYSIS

Light absorption by the electrolyte introduces an efficiency loss by reducing the irradiance at the photoelectrode. An analysis was performed to determine the magnitude of this loss as a function of absorbance path length.

In the following text, data will be presented to show the effects of electrolyte light absorption for path lengths between 0.5 and 10 mm. The spectral results were obtained with a Perkin-Elmer model 356 spectrophotometer equipped with 1 millimeter path length cuvettes. The Lambert-Beer absorption law was then applied to calculate an absorbance spectrum for the following path lengths: 0.5, 2, 5 and 10 mm. (The Lambert-Beer law states that absorbance is directly proportional to path length). The absorption spectra were mathematically converted to equivalent transmission curves which in turn were used to calculate a new spectral irradiance level for the appropriate

TABLE X

Laser Probe Response of Photoelectrochemical Cells 8, 9 and 10 - Series C

	Vertical Position (VP)				
	1	2	3		
CELL 8	10.7 –	10.2 –	10.8 –	1	HORIZONTAL POSITION (HP)
	12.8 –	10.8 –	11.2 –	2	
	16.1 –	13.6 –	17.1 –	3	
	7.9 –	15.5 –	12.6 –	4	
	7.9 –	6.8 –	8.9 –	5	
	1	2	3		
CELL 9	141.6 0.70	134.8 0.66	138.2 0.68	1	
	150.3 0.80	94.3 0.40	149.9 0.80	2	
	138.5 0.72	88.5 0.36	127.2 0.62	3	
	147.0 0.80	90.6 0.40	149.0 0.84	4	
	136.7 0.66	128.7 0.60	129.0 0.60	5	
	1	2	3		
CELL 10	44.4 0.46	42.9 0.44	39.8 0.40	1	
	46.3 0.48	47.0 0.50	47.2 0.50	2	
	45.8 0.48	46.8 0.50	47.7 0.52	3	
	44.0 0.46	48.0 0.52	46.5 0.50	4	
	44.1 0.46	43.4 0.46	41.0 0.42	5	

Eg. Cell 9 position VP-1, HP-1

Open-Circuit Voltage: 141.6 mV
Short-Circuit Current: 0.70 mA

path length. In order to improve the accuracy in the region of weaker absorption a spectrum was recorded with 10 mm path length cuvettes. Within experimental error, the absorbance levels were 10 times those obtained with the 1 mm cuvettes. The data from the 10 mm path length spectrum was used in the region of weaker absorption.

The one millimeter path length absorption spectrum for 1M polysulphide electrolyte can be seen in Figure 24 while the calculated transmission curves for path lengths of 0.5, 1, 2, 5 and 10 mm appear in Figure 25. The effect of electrolyte light absorption on incident AM1 irradiation can be seen in Figure 26. As the absorption path length increases the spectral distribution is red-shifted, that is to say, increasing amounts of radiation in the 300 to 500 nm range are absorbed. Referring to Figure 26 again, the vertical line at 730 nm corresponds to the absorption edge of CdSe, and as mentioned earlier, only radiation of wavelengths shorter than this can promote electrons from the valence band to the conduction band. The irradiation losses induced by electrolyte absorption were quantified by comparing the areas under the curves up to the absorption edge wavelength (300 to 730 nm range). The area under the curve for AM1 corresponds to an irradiance level of 46.6 mW/cm^2. When AM1 radiation passes through 0.5 mm of electrolyte the irradiance level is reduced to 30.1 mW/cm^2 or expressed as a percentage, 64.7% of the radiation is reaching the photoelectrode. Similar results are presented for absorbance path lengths of 1, 2, 5 and 10 mm in Figure 27. Based upon the terrestrial intensity (88.9 mW/cm^2), approximately 23% of the radiation is absorbed while passing through 2 mm of polysulphide electrolyte (the photoelectrodes of the Series C cells were 2 mm from the plexiglas housing).

In the following text, three electrolyte-related observations will be reported. First, the stability of the polysulphide electrolyte was qualitatively examined. The stability of the polysulphide electrolyte is affected by exposure to the atmosphere, particularly oxygen and carbon dioxide. Figure 28 shows the deterioration of the polysulphide electrolyte over a 4 week period. The transmission increases due to the loss of the absorbing species - the polysulphide. Secondly, early in the evaluation, it was postulated that the poor electrical performance exhibited by some cells might be the result of the formation of a depletion zone of oxidized polysulphide in the space between the photoelectrode and the plexiglas housing. This theory was proven invalid when no improved performance was observed with electrolyte circulation. The electrolyte was circulated at a rate of 100 mls/minute, a rate that exchanged the electrolyte in the space between the photoelectrode and the plexiglas housing 50 times per minute. The third electrolyte-related observation pertains to electrolyte temperature. Several cells were operated at maximum power output under AM1 illumination for a period of 3 hours. A stable electrolyte temperature of 30 to 35°C was recorded.

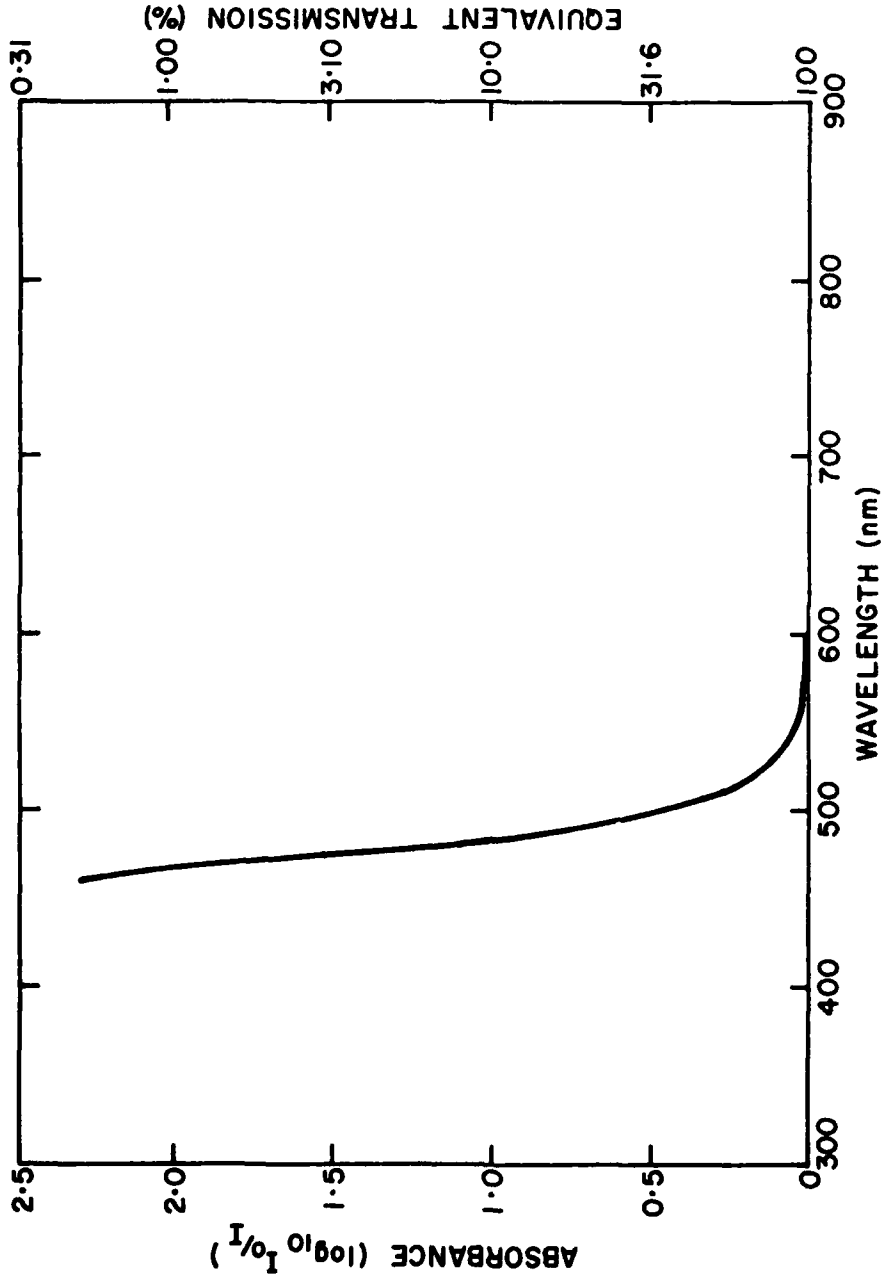

Fig. 24: Absorption spectrum of 1 M polysulphide electrolyte. (One millimeter path length).

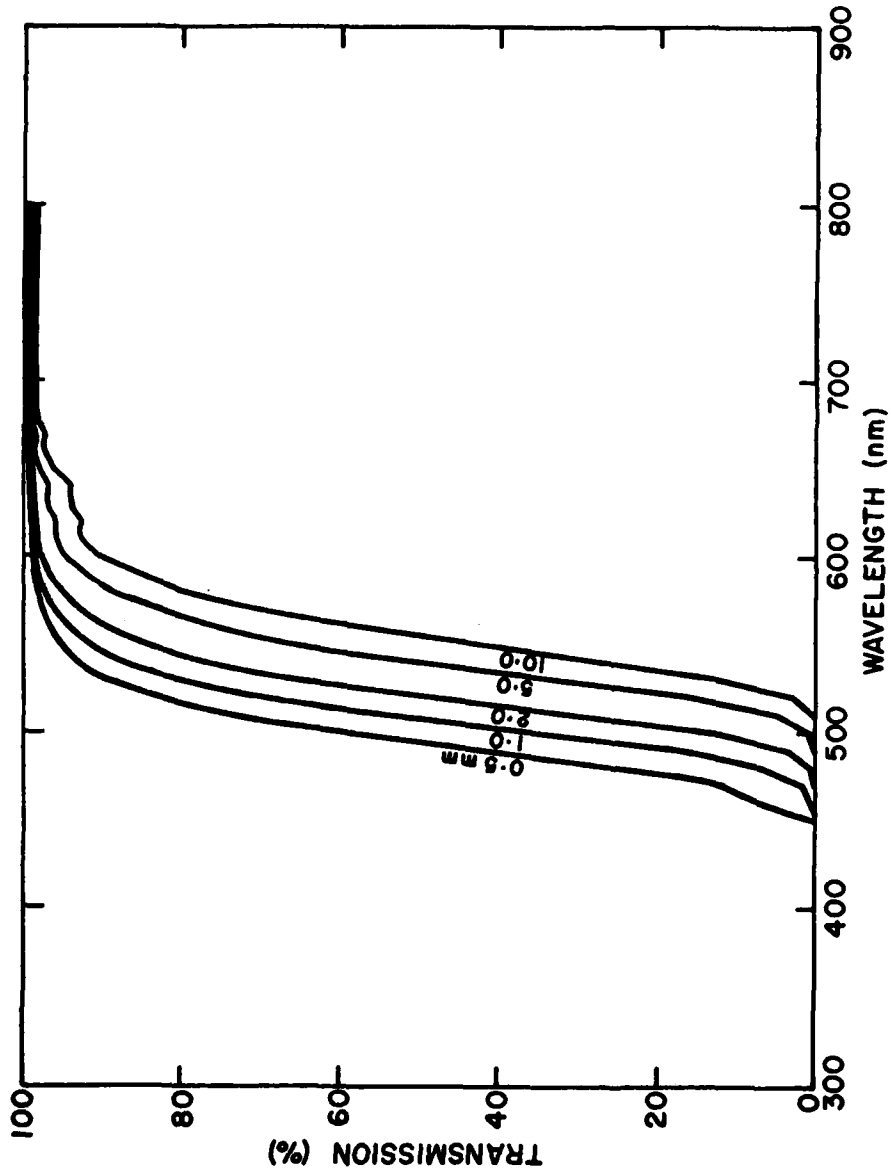

Fig. 25: Spectral transmission of the polysulphide electrolyte for path lengths of 0.5, 1, 2, 5 and 10 millimeters.

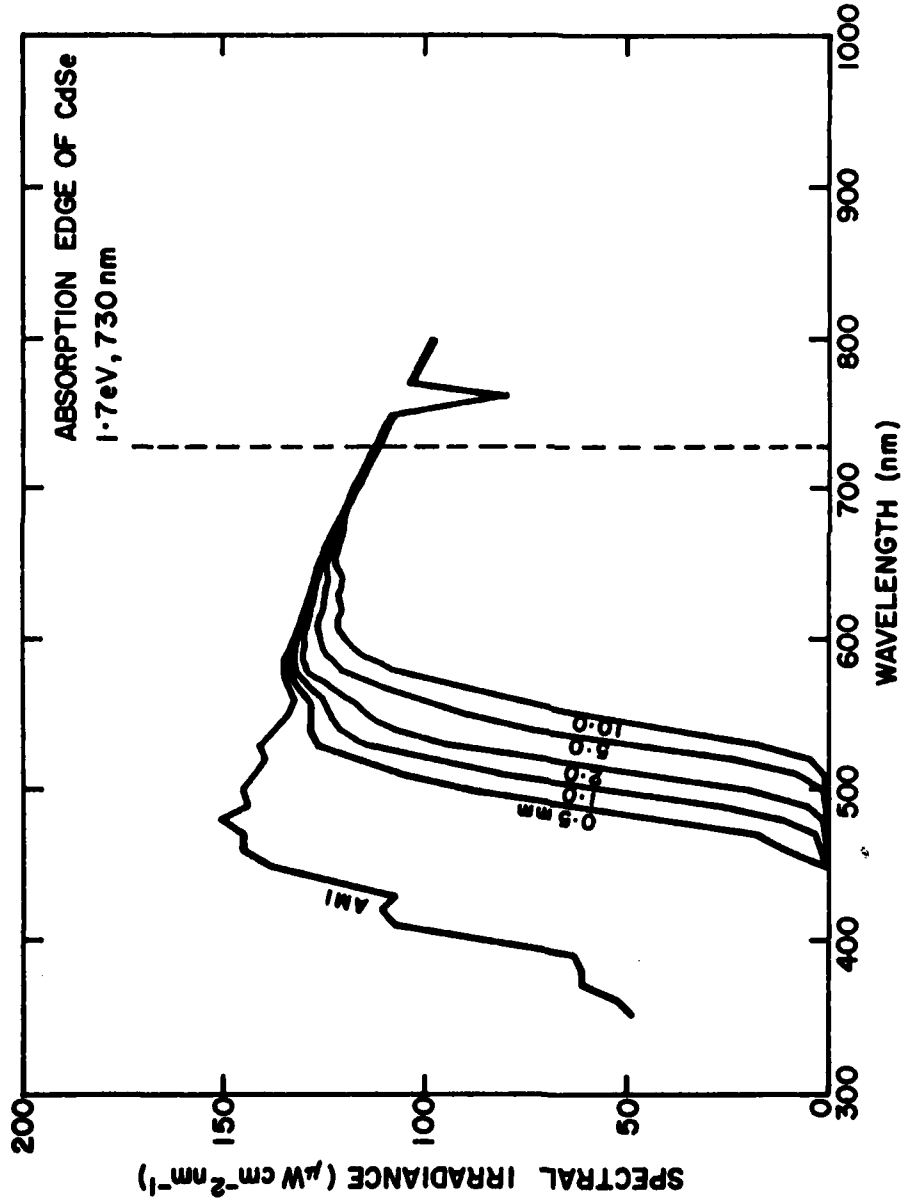

Fig. 26: The effect of electrolyte light absorption on incident AMI radiation.

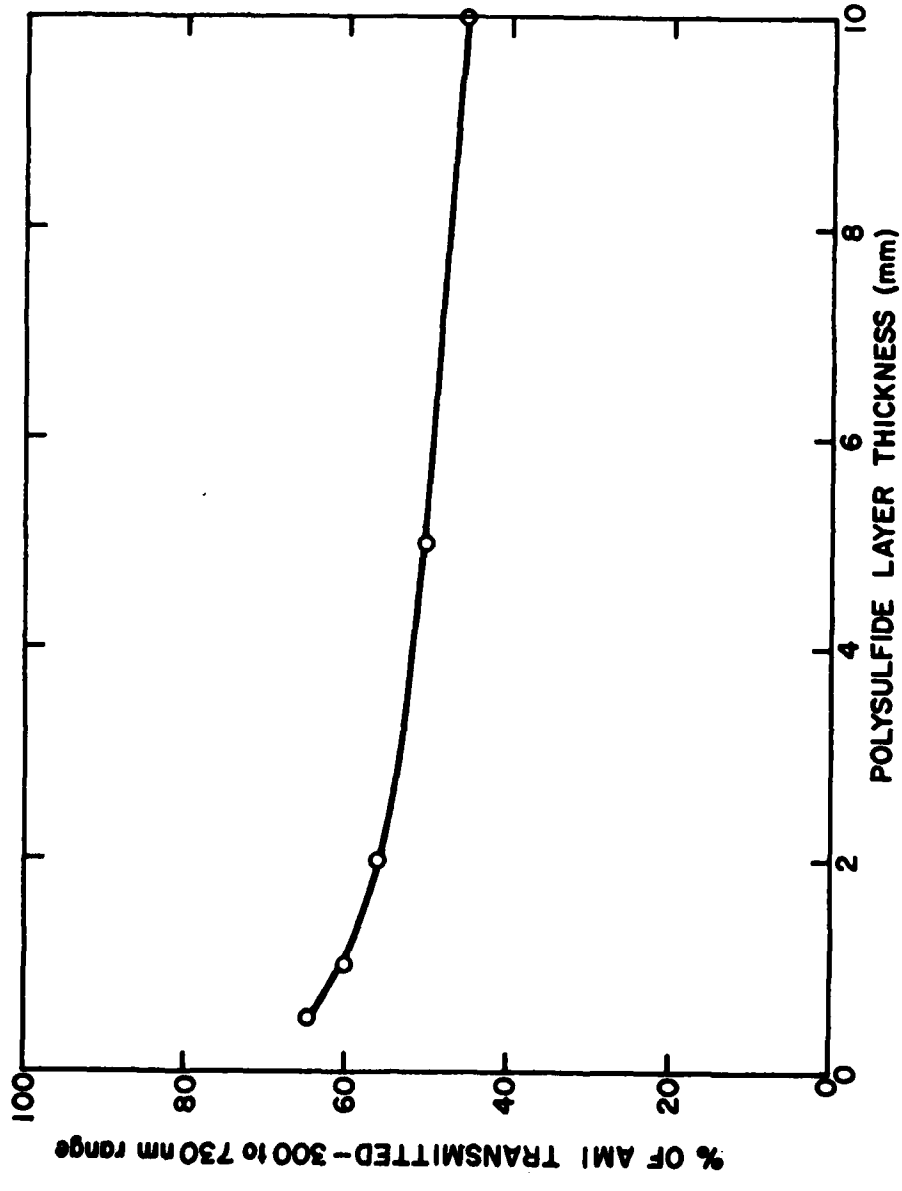

Fig. 27: The effect of electrolyte light absorption on irradiance levels in the band-gap region (300 to 730 nm) of CdSe photoelectrochemical cells.

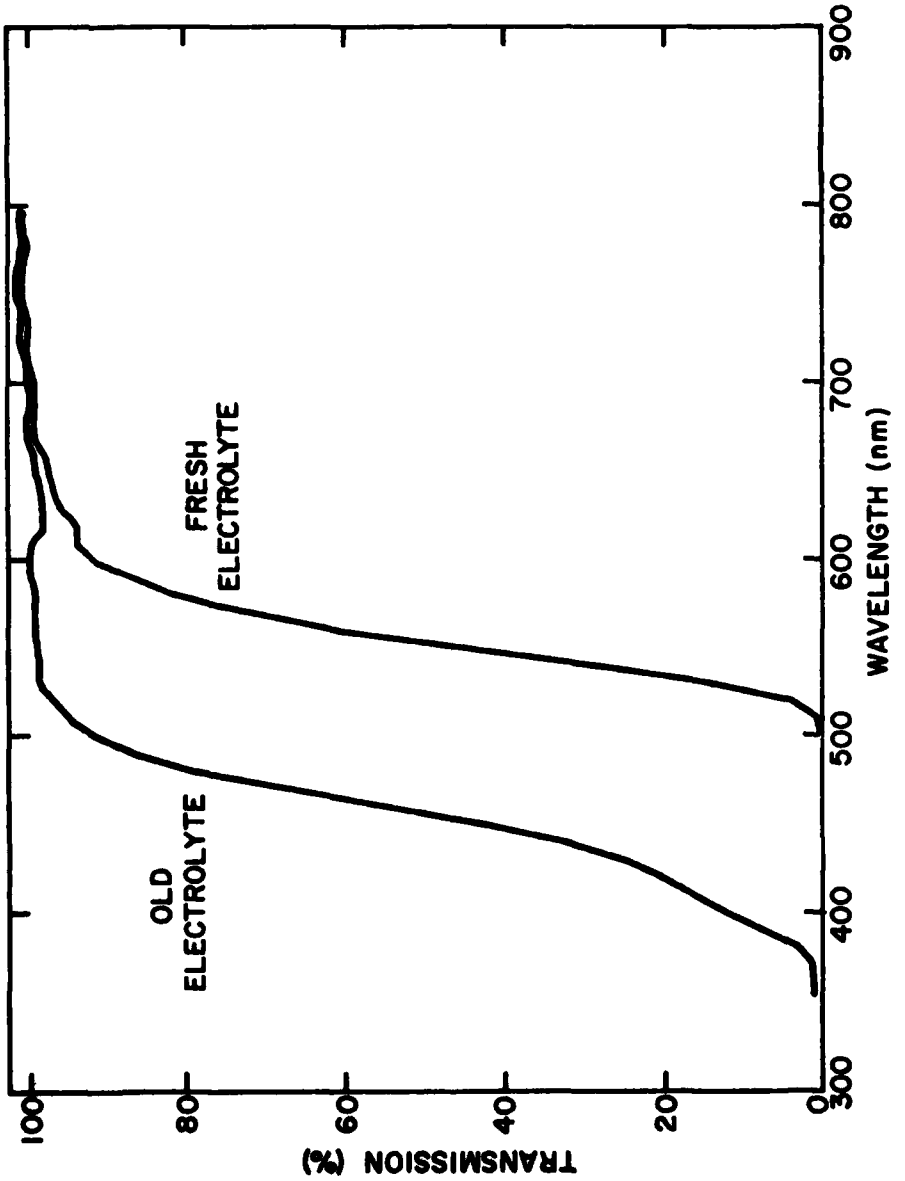

Fig. 28: Electrolyte deterioration.

DISCUSSION

The current-voltage characteristics of all the cells tested (Figs. 3-6,8,9,11,15 and 16) show similar behaviour in that the observed voltage falls off approximately linearly with current. This behaviour is in contrast to the results obtained with single crystal [6] or with pressure sintered [7] cadmium selenide photoelectrodes immersed in 1M polysulphide electrolyte, which show a much slower drop in output voltage with increasing current density. The behaviour observed here is similar to that observed with other electrochemically deposited CdSe electrodes [8]. The maximum open-circuit voltages recorded ($\leq$ 350 mV) are approximately one-half the corresponding values for single crystal CdSe [6] or pressure sintered CdSe [7]. For slightly lower irradiance levels (approximately AM2 levels) the short-circuit currents obtained with single crystal and pressure sintered materials [6,7] are at least twice and more commonly five times the values recorded for the CdSe photoelectrodes examined at DREO.

The shape of the current-voltage curves can be quantified by calculating the fill-factor, which is defined as:

$$\text{Fill-Factor} = \frac{P_{OUT}}{I_{SC} \times V_{OC}}$$

where I_{SC} and V_{OC} are the observed short-circuit current and open-circuit voltage, respectively. P_{OUT} is the maximum observed output power. Clearly the fill-factor must be less than or equal to 1, and for a cell whose output voltage drops off linearly with current, the fill-factor will be 0.25. Fill-factors of 0.7 to 0.8 have been recorded for silicon photocells, 0.57 and 0.45 for single crystal and pressure sintered CdSe photoelectrodes, respectively [9]. Since the output voltage varies linearly with current for the photoelectrodes examined at DREO, the fill-factor is 0.25.

Thus even the best of the electrodeposited CdSe photoelectrodes have V_{OC}, I_{SC} and fill-factors which are approximately one-half those observed with single crystal and pressure sintered CdSe. Since the power output is the product of these three factors, the efficiency of the electrodeposited materials is an order of magnitude less than other materials. In order to improve the conversion efficiency of the electrodeposited CdSe photoelectrodes we must identify and correct the cause of these losses.

The behaviour of heterojunction and Shottky barrier junction photocells can be represented, to a first approximation, by the equivalent circuit

shown in Figure 29 [10]. V_L and I_L are the voltage and current associated with the load resistance R_L, I_p is the photo-generated current and I_D is the diode current which is a function of V_i. Since I_D is a function of V_i, the equation shown in Figure 29 must be solved numerically. Although the CdSe photoelectrochemical cells are analogous to Shottky barrier photodiodes, the circuit shown in Figure 29 is not an exact representation [10], but in general it can be seen that the diode shunt resistance (R_{SH}) should be high and the series resistance (R_S) should be low. Both the solution resistance and the CdSe resistance can contribute to R_S which should be less than 0.5Ω for efficient operation. The current-voltage characteristics of the cells reported on can be attributed to a series resistance of a few ohms, resulting in rapid voltage loss with increasing current density.

Heller and co-workers [7,11,12], using a two beam spectroscopic technique, have shown that states at or near the semiconductor/liquid interface can act as recombination centers. (The presence of these states correlates with reduced V_{OC}, I_{SC} and fill-factors for both single crystal and polycrystalline CdSe.) These recombination centers act by trapping the current carriers and thus delaying their separation. The corresponding increased concentration of minority and majority current carriers leads to a more rapid rate of recombination and hence saturation, i.e. the photocurrent no longer increases with irradiance [11]. Before saturation occurs, there will of course be a decrease in photocurrent due to these recombination states. Such a saturation effect can be seen in the results shown in Figure 21 although there are alternative explanations which will be discussed below. For the single crystal and pressure sintered CdSe the recombination centers can be removed by an acid etch, however, it is not clear that the electrodeposited photoelectrodes would survive such treatment.

A further cause of degradation in photoelectrode performance is the presence of surface states produced by surface defects or absorbed impurities [12,13]. If these states fall between the conduction and valence bands as shown in Figure 30, then the maximum photovoltage which can be developed (V_{OC}) may decrease. The conduction band tends to flatten out under increased illumination, and in the absence of surface states, the maximum output voltage would be developed at the flat band condition. However, before this condition is reached the electrons may tunnel to a surface state thus acting as a shunt, limiting the V_{OC} and the fill-factor. It has been pointed out [12] that if a strongly chemisorbed impurity is added, the surface state will be lowered to the point where the barrier is too thick for tunneling to occur. Thus weakly absorbed impurities which could cause deterioration in performance are excluded. The n-type GaAs photoanodes treated with Ru^{3+} solution show a marked increase in efficiency [12]. Use of this technique for improving the performance of electrodeposited CdSe has not so far been reported.

Although many of the causes of degradation in photocell performance are speculative, polarization at the counter electrode was definitely identified as one contributing effect. The results shown in Table IX and Figures 18 and 19 indicate that counter electrode polarization amounting to 65-70% of the V_{OC} occurs at short-circuit conditions. This polarization, which declines with decreasing light intensity, provides an explanation of the saturation observed in Figure 21 at higher intensities. Thus improvements

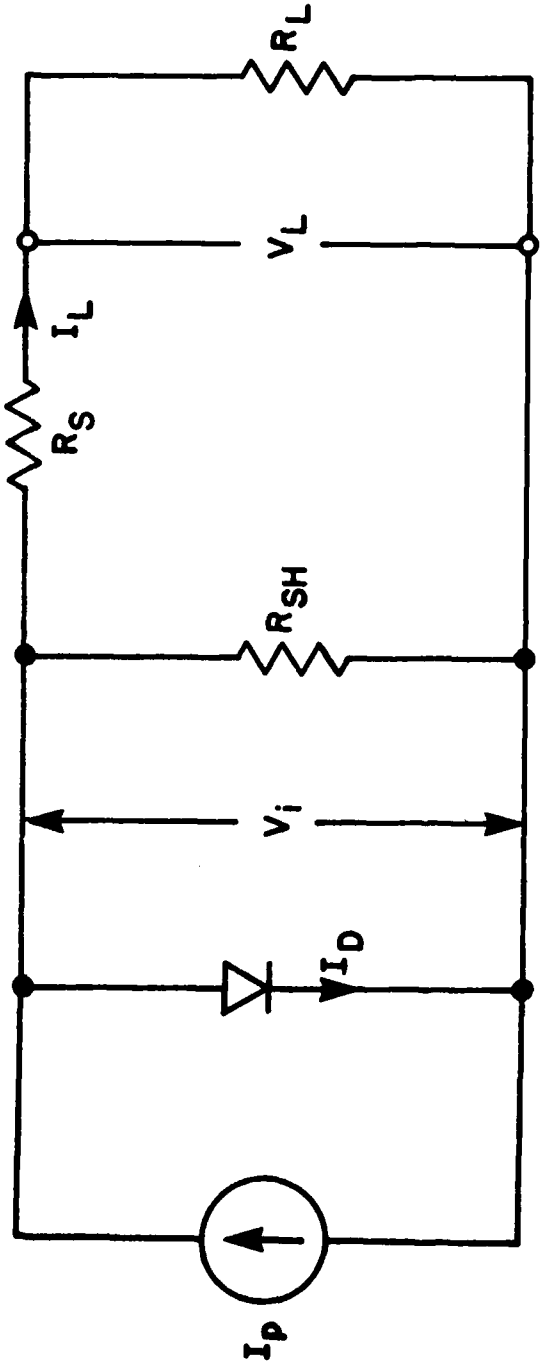

$$I_L(1 + R_S/R_{SH}) = I_p - I_D(V_i) - V_L/R_{SH}$$

Fig. 29: Simple equivalent circuit of a Solar Cell.

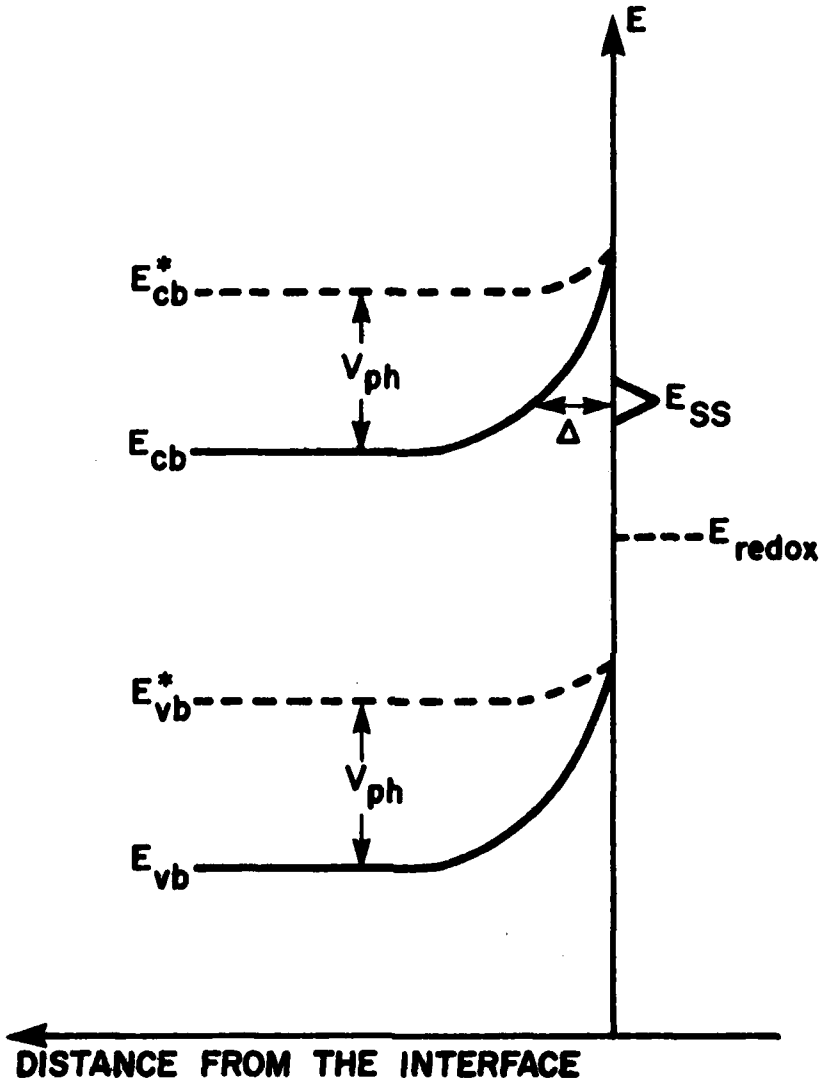

Fig. 30: Energy diagram showing the conduction band (cb), valence band (vb), surface state (ss), and redox level for illuminated (dashed line) and dark conditions (solid lines). V_{ph} is the photo voltage developed.

in the counter electrode performance are clearly required. It is not clear if the "Grafoil" carbon electrodes of the Series C cells were treated with cobalt salts as for the earlier A and B Series [1]. CoS clearly provides a material for which the overpotential is very low [14] (30 mV for a current density of 5 mA/cm^2), much lower than the values we have measured. Counter electrodes having very low polarizations have been successfully fabricated [14,15].

A further loss process which can be readily quantified is the absorption of light in the polysulphide electrolyte. The polysulphide absorption spectrum is shown in Figure 25 and the spectrum of transmitted AM1 sunlight in Figure 26. This result, which was used to calculate the fractional transmission of AM1 sunlight through various path lengths of polysulphide electrolyte as shown in Figure 27, indicates that for the 2 to 3 mm path length typical of the cells tested, approximately 55% of the light is transmitted. The shape of Figure 27 is interesting in that it shows that the losses are not linear with increasing path length. Approximately 35% of the light is lost in the first 0.5 mm and for a 5 mm path length this loss has only increased to 50%. Thus providing a path length of the order of 2 mm is to be tolerated (shorter path lengths than this would probably be impractical in a large area photocell) very little extra losses are incurred in increasing the path lengths to 5 or even 10 mm. The transmission of the polysulphide solution for tungsten filament radiation such as that shown in Figure 6 is somewhat greater. For example, using the spectral distribution of Figure 6, the calculated transmission of radiation in the 300-730 nm wavelength band is 79% compared to 56% for AM1 radiation (Figure 27). This increase in transmission, which results from the red-shifted filament light source, can contribute to apparently increased efficiencies using these light sources.

In summarizing the above discussions it should be noted that although the effects of electrode polarization and light absorption by the electrolyte have been quantified, the contribution of series resistance in the semiconductor bulk, surface states, electron-hole recombination centers, and shorting to the Ni substrate as mechanisms for a loss in performance are speculative. This points to the need for further research to identify and characterize these mechanisms. In particular the technique of two beam photocurrent spectroscopy [7,12], which has not been applied to electrodeposited materials, would be very useful for probing recombination centers that fall in the depletion region. It would also be very useful to characterize the CdSe layer. Although it is clear that the CdSe is n-type material and that the "dopant" is Cd (see for example ref. 2) the conductivity of the material is unknown. Attempts to measure both the donor concentrations and the flat-band potential from Mott-Schottky plots have proved unsuccessful [2]. This has tentatively been attributed to shorting of the small space-charge layer capacitance by the much larger Helmholtz layer capacitance due to shorting of the CdSe layer by direct contact of the Ni substrate with the electrolyte.

Another measure of performance which can be useful is the efficiency of electron production (η). η is the ratio of electrons produced (at short-circuit current conditions) to photons incident on the electrode. As an example we can take the maximum short-circuit current observed for a series C cell of 22 mA (Table VII) with light source 3-2. The number of photons incident on the 10 cm^2 photoelectrode was calculated by converting the

spectral irradiance (I) of Figure 14 to N (photons/cm^2-nm-sec) using the relationship:

$$N = \frac{I \times 10^{-6}}{h \times c} \lambda \times 10^7$$

where λ is wavelength in cm, h is Planck's constant in units of erg-sec and c is the velocity of light in cm/sec. The function N was then numerically integrated from 300 to 730 nm to give the total number of photons/cm^2-sec in this wavelength range. The number of photons incident on a 10 cm^2 surface is 1.2×10^{18} which gives η a value of 12%. Although losses attributable to surface reflections and absorption in the electrolyte can account for a part of this low efficiency it is evident that there is considerable loss of electron-hole pairs due to recombination before they can be separated. For an AM1 source there are 1.3×10^{17} photons/cm^2-sec in the 300-730 nm wavelength band and if we assume that 60% of these photons are transmitted by the solution we obtain a maximum short circuit current of 12 mA/cm^2.

Although no specific long term testing of the stability of the photoelectrodes was undertaken it is clear from the data presented that there was a steady degradation in performance. This was expected from the results obtained by other groups [6,12,16] and apparently results from substitution of S for Se in the surface layer. It has been suggested that this leads to a CdSe/CdS heterojunction which blocks the flow of holes to the surface [12]. Furthermore, with increasing substitution of S for Se the band gap of the electrode will approach that of CdS (5200 Å). If we compare this threshold wavelength with the spectra of an AM1 source after transmission through various thicknesses of polysulphide electrolyte (Figure 26) we can see that there is, at most, a very narrow transmission window between the cut-on due to electrolyte transmission and the cut-off due to the band-gap. In fact a CdS photoelectrode in the polysulphide electrolyte has a very low potential efficiency.

Not only has the mechanism of CdSe photoelectrode instability been identified but a method of alleviating the problem has been found [6]. Addition of as little as 0.01M Se to the polysulphide electrolyte leads to greatly increased photoelectrode lifetime. With a Se concentration of 0.05M a total charge of greater than 2×10^4 C/cm^2 could be extracted [6] before signs of deterioration were detected. At 20 mA/cm^2 this corresponds to a lifetime greater than 10^6 hours. Thus we feel that future research should identify the optimum amount of Se and future photoelectrochemical cells should include Se in the electrolyte. The Se containing solution shows increased optical absorption, therefore the stabilizing effect is obtained at the price of decreased optical transmission.

An examination of the results on the efficiency of the storage component of the cells, which are summarized in Table VI, indicate that the poor efficiency can be attributed to a high charging potential. Thus, although the Ag/Ag_2S couple with its potential of 210 mV [8] can theoretically be charged by a single photoelectrode further research efforts are required to reduce the overvoltage in order to make this practical. Because of the cost of silver it will undoubtedly be necessary to find a substitute for Ag in any practical device and thus research efforts are perhaps better directed

at developing cheaper alternative storage electrodes.

CONCLUSIONS AND RECOMMENDATIONS

Although the photoelectrochemical cell comprised of an electrochemically deposited CdSe photoelectrode in a polysulphide electrolyte continues to show promise it is clear that many problems remain to be solved before its full potential can be evaluated. Increased research effort is required in order to characterize the bulk CdSe and the structure of the depletion layer and the CdSe/electrolyte interface.

The polysulphide electrolyte is far from ideal, both because of its optical absorption and because of its sensitivity to the atmosphere. This sensitivity to oxidation and the associated problems of CO_2 absorption by the alkaline electrolyte will require a practical device to be hermetically sealed, thus posing fabrication problems. Long-term stabilization of the CdSe photoelectrodes in the polysulphide remains a problem, although, as noted above, addition of elemental selenium greatly decreases the CdSe photocorrosion. In spite of these deficiencies the polysulphide appears to be the best redox electrolyte currently available.

Because of the high cost of Ag the in situ storage of energy using the Ag/Ag_2S couple will not be economically viable. Thus a research effort directed at developing a cheaper alternative rather than solving the problems with the Ag/Ag_2S couple would be more appropriate.

The appropriateness of developing CdSe photoelectrochemical devices before the interfering problems which limit performance are resolved can be questioned. Nevertheless, the co-operative effort between the groups at Simon Fraser University and DREO has helped DREO achieve an expertise in what was a new area of research. The continuing exchange of information has also greatly assisted the general development of research on photoelectrochemical cells in both groups.

Continuing research and development in this area should be directed along the following lines:

1. Experimental techniques such as two-beam photocurrent spectroscopy should be applied to the electrochemically deposited CdSe in order to detect the presence of surface states and electron-hole recombination centers that can lead to degradation of performance.

2. Techniques must be found and applied to evaluate the bulk properties of the CdSe. For example, properties such as the structure, doping levels, conductivity as well as the flatband potential must be measured. Experimental procedures for controlling the doping and annealing of the CdSe can then be

evaluated. The failure of capacitance data on electrochemically deposited CdSe to provide much of this information via Mott-Shottky plots must be examined.

3. Exposure of pressure sintered CdSe and Cd vapour during annealing was found to be essential in order to obtain efficient operation [9]. Evaluation of annealing procedures for electrochemically deposited CdSe both with and without Cd treatment is required.

4. Increased photoelectrode stability must be achieved and demonstrated. Techniques such as chemical derivatization (eg. chemically bonding selected redox couples to the surface) may be useful both to mediate charge transfer and to protect the surface.

5. A lower cost storage couple than the Ag/Ag_2S should be sought.

In summary, several research problems remain to be solved before the CdSe photoelectrochemical cell, with or without in situ storage, could be developed into devices which will be able to compete with existing technology such as n-p junction silicon solar cells coupled with battery storage. No fundamental impediment to such development has been uncovered in this work and photoconversion efficiencies of 5-10% should be possible. Efficiencies in this range will undoubtedly be required if these cells are going to be economic.

REFERENCES

1. Final report to Department of Supply and Services on Contract No. 2SU77-00346, April 1978, B.L. Funt and M. Leban.

2. Final report to Department of Supply and Services on Contract No. 8SU77-00433 by B.L. Funt, January 1979.

3. M.P. Thekaekara, in Solar Energy Engineering, Edited by A.A.M. Sayigh, Academic Press, New York, 1977.

4. H. Brandhorst et al., Interim solar cell testing procedures for terrestrial applications, NASA TM-X-71771, NASA, Lewis Research Center, Cleveland, Ohio (1975).

5. R.A. Sawchuk and D.R. Snelling, in preparation.

6. A. Heller, G.P. Schwartz, R.G. Vadimsky, S. Menezes and B. Miller, J. Electrochem. Soc., 125, 7, 1156-1160 (1978).

7. A. Heller, K.C. Chang and B. Miller, J. Electrochem. Soc., 124, 5, 697-700 (1977).

8. G. Hodes, J. Manassen and D. Cahen, Nature, 261, 403-404 (1976).

9. B. Miller, A. Heller, M. Robbins, S. Menezes, K.C. Chang and J. Thomson, Jr., J. Electrochem. Soc., 124, 7, 1019-1021 (1977).

10. David L. Pulfrey, Photovoltaic Power Generation, Van Nostrand Reinhold Company, New York, N.Y., p 70 (1978).

11. A. Heller, K.C. Chang and B. Miller, J. Amer. Chem. Soc., 100, 3, 684-688 (1978).

12. A. Heller and B. Miller, Electrochimica Acta, in print.

13. B.A. Parkinson, A. Heller and B. Miller, J. Electrochem. Soc., 126, 6, 954-960 (1979).

14. J.R. Owen and W.A. Gerrard, "A Novel Electrochemical Solar Cell", in Photovoltaic Solar Energy Conference, Proceedings of the International Conference, Luxembourg, Sept. 27-30, 1977, pp 436-444, D. Reidel Publishing Company, Inc., Holland, 1978.

15. Y. Auigal, D. Cahen, J. Manassen and G. Hodes, "Solar Energy Conversion and Storage by a Photoelectrochemical Solar Cell", ibid., pp 1302-1322.

16. D. Cahen, G. Hodes and J. Manassen, J. Electrochem. Soc., 125, 10, 1623-1628 (1978).

UNCLASSIFIED

Security Classification

DOCUMENT CONTROL DATA - R & D

(Security classification of title, body of abstract and indexing annotation must be entered when the overall document is classified)

1. ORIGINATING ACTIVITY Defence Research Establishment Ottawa Department of National Defence Ottawa, Ontario K1A 0Z4	2a. DOCUMENT SECURITY CLASSIFICATION UNCLASSIFIED 2b. GROUP N/A

3. DOCUMENT TITLE

INVESTIGATION OF CADMIUM SELENIDE PHOTOELECTROCHEMICAL CELLS

4. DESCRIPTIVE NOTES (Type of report and inclusive dates)

TECHNICAL NOTE

5. AUTHOR(S) (Last name, first name, middle initial)

SAWCHUK, Robert A. and SNELLING, David R.

6. DOCUMENT DATE	7a. TOTAL NO OF PAGES	7b. NO OF REFS
JANUARY 1980	60	16

8a. PROJECT OR GRANT NO	9a. ORIGINATOR'S DOCUMENT NUMBER(S)
	DREO TECHNICAL NOTE NO. 80-4
8b. CONTRACT NO	9b. OTHER DOCUMENT NO (S) (Any other numbers that may be assigned this document)

10. DISTRIBUTION STATEMENT

UNLIMITED DISTRIBUTION

11. SUPPLEMENTARY NOTES	12. SPONSORING ACTIVITY

13. ABSTRACT

Three photoelectrochemical devices, developed at Simon Fraser University, employing electrochemically deposited cadmium selenide photoanodes, a polysulphide redox electrolyte, and an in situ energy storage compartment were evaluated at DREO. A simulated solar source (AM1) was designed and built to evaluate these and other devices.

Maximum power output of the devices was in the 10 to 20 mW range resulting in a solar (AM1) to electrical conversion efficiency of less than 1%. The efficiency was limited by counter electrode polarization, electrolyte light absorption and photocurrent losses originating in the semiconductor bulk or the depletion region.

It is concluded that further research is required to characterize both the polycrystalline semiconductor phase and the semiconductor/electrolyte interface. An appreciation of the potential of photoelectrochemical devices is offered in the Conclusions and Recommendations section of this report.

UNCLASSIFIED

DSIR

77-865

KEY WORDS

PHOTOELECTROCHEMICAL CELL

SOLAR CELL

CADMIUM SELENIDE

POLYSULPHIDE

ELECTROCHEMICAL DEPOSITION

ENERGY STORAGE

EVALUATION

INSTRUCTIONS

1. ORIGINATING ACTIVITY: Enter the name and address of the organization issuing the document.

2a. DOCUMENT SECURITY CLASSIFICATION: Enter the overall security classification of the document including special warning terms whenever applicable.

2b. GROUP: Enter security reclassification group number. The three groups are defined in Appendix 'M' of the DRB Security Regulations.

3. DOCUMENT TITLE: Enter the complete document title in all capital letters. Titles in all cases should be unclassified. If a sufficiently descriptive title cannot be selected without classification, show title classification with the usual one-capital letter abbreviation in parentheses immediately following the title.

4. DESCRIPTIVE NOTES: Enter the category of document, e.g. technical report, technical note or technical letter. If appropriate, enter the type of document, e.g. interim, progress, summary, annual or final. Give the inclusive dates when a specific reporting period is covered.

5. AUTHOR(S): Enter the name(s) of author(s) as shown on or in the document. Enter last name, first name, middle initial. If military, show rank. The name of the principal author is an absolute minimum requirement.

6. DOCUMENT DATE: Enter the date (month, year) of Establishment approval for publication of the document.

7a. TOTAL NUMBER OF PAGES: The total page count should follow normal pagination procedures, i.e., enter the number of pages containing information.

7b. NUMBER OF REFERENCES: Enter the total number of references cited in the document.

8a. PROJECT OR GRANT NUMBER: If appropriate, enter the applicable research and development project or grant number under which the document was written.

8b. CONTRACT NUMBER: If appropriate, enter the applicable number under which the document was written.

9a. ORIGINATOR'S DOCUMENT NUMBER(S): Enter the official document number by which the document will be identified and controlled by the originating activity. This number must be unique to this document.

9b. OTHER DOCUMENT NUMBER(S): If the document has been assigned any other document numbers (either by the originator or by the sponsor), also enter this number(s).

10. DISTRIBUTION STATEMENT: Enter any limitations on further dissemination of the document, other than those imposed by security classification, using standard statements such as

(1) "Qualified requesters may obtain copies of this document from their defence documentation center."

(2) "Announcement and dissemination of this document is not authorized without prior approval from originating activity."

11. SUPPLEMENTARY NOTES: Use for additional explanatory notes.

12. SPONSORING ACTIVITY: Enter the name of the departmental project office or laboratory sponsoring the research and development. Include address.

13. ABSTRACT: Enter an abstract giving a brief and factual summary of the document, even though it may also appear elsewhere in the body of the document itself. It is highly desirable that the abstract of classified documents be unclassified. Each paragraph of the abstract shall end with an indication of the security classification of the information in the paragraph (unless the document itself is unclassified) represented as (TS), (S), (C), (R), or (U).

The length of the abstract should be limited to 20 single-spaced standard typewritten lines, 7½ inches long.

14. KEY WORDS: Key words are technically meaningful terms or short phrases that characterize a document and could be helpful in cataloging the document. Key words should be selected so that no security classification is required. Identifiers, such as equipment model designation, trade name, military project code name, geographic location, may be used as key words but will be followed by an indication of technical context.